ABSTRACT

Title of Thesis: EVALUATION OF AN EXTENDED DUCT AIR DELIVERY SYSTEM FOR SPACES CONDITIONED BY ROOFTOP UNITS

Ryan Kennett, Master of Science, 2016

Thesis Directed By: Research Professor Yunho Hwang, Ph.D.
Department of Mechanical Engineering

Traditional air delivery to high-bay buildings involves ceiling level supply and return ducts that create an almost-uniform temperature in the space. Problems with this system include potential recirculation of supply air and higher-than-necessary return air temperatures. A new air delivery strategy was investigated that involves changing the height of conventional supply and return ducts to have control over thermal stratification in the space. A full-scale experiment using ten vertical temperature profiles was conducted in a manufacturing facility over one year. The experimental data was utilized to validated CFD and EnergyPlus models. CFD simulation results show that supplying air directly to the occupied zone increases stratification while holding thermal comfort constant during the cooling operation. The building energy simulation identified how return air temperature offset, set point offset, and stratification influence the building's energy consumption. A utility bill analysis for cooling shows 28.8% HVAC energy savings while the building energy simulation shows 19.3 – 37.4% HVAC energy savings.

EVALUATION OF AN EXTENDED DUCT AIR DELIVERY SYSTEM FOR SPACES CONDITIONED BY ROOFTOP UNITS

by

Ryan Kennett

Thesis submitted to the Faculty of the Graduate School of the
University of Maryland, College Park, in partial fulfillment
of the requirements for the degree of
Master of Science
2016

Advisory Committee:
Research Professor Yunho Hwang, Chair
Professor Jelena Srebric
Associate Professor Bao Yang

Acknowledgements

I would like to gratefully acknowledge the support of the following people and organizations, without whom this research would not have been possible. My advisor Dr. Yunho Hwang for sharing his knowledge, guidance, and vision over the past two years. Jan Muehlbauer for his skills in the lab and information you can't find anywhere else. XChanger Co. for their ideas, enthusiasm, and product. Holmatro Inc. and John Freeburger for being welcoming and helpful during our measurement setup. Maryland Industrial Partnership Program (MIPS) for facilitating this unique collaboration. Dr. Reinhard Radermacher and Dr. Hoseong Lee for their consistently insightful feedback during weekly meetings. And finally, my fellow researchers and friends at CEEE for their daily support and motivation.

Table of Contents

Acknowledgements ii

Table of Contents iii

List of Tables vi

List of Figures viii

Nomenclature xi

1. Introduction 1

    1.1 Motivation 1

    1.2 Conventional Air Delivery Strategy for High Bay Buildings 2

    1.3 Proposed Air Delivery System 4

    1.4 Objective 7

2. Experimental Work 7

    2.1 Test Facility 7

    2.2 Literature Review 10

    2.3 Instrumentations and Data Acquisition 13

    2.4 Uncertainty Analysis 15

3. Computational Fluid Dynamics Modeling 16

    3.1 Literature Review 16

    3.2 Objective 21

    3.3 Governing Equations and Turbulence Modeling 22

    3.4 Geometry and Computational Grid 23

3.5 Solver Settings 28
3.6 Boundary Conditions 29
4. Building Energy Simulation 32
4.1 Literature Review 32
4.2 Room Air Modeling 35
4.3 Weather Data 44
4.4 Schedules 45
4.5 Electrical and Thermal Loads 47
4.5.1 Electrical Equipment 47
4.5.2 Lights 48
4.5.3 Occupants 49
4.6 Building Envelope and Surface Constructions 49
4.6.1 Outer Walls 49
4.6.2 Interior Walls and Open Doorways 50
4.6.3 Floor 51
4.6.4 Roof Construction 51
4.7 Primary Systems (RTUs and air delivery) 52
4.7.1 Cooling Coil 53
4.7.2 Heating Coil 56
4.7.3 Economizer Control 56
4.7.4 Fans 58

4.8 Infiltration 60
4.9 Retrofit Modeling 62
4.9.1 Lights 62
4.9.2 Rooftop Units 63
4.9.3 Air Compressor 64
5. Results Analysis and Discussion 66
5.1 Experiment 66
5.1.1 Temperature Profiles 66
5.1.2 Utility Bill Analysis 70
5.2 CFD Modeling 78
5.2.1 Grid Sensitivity Analysis 78
5.2.2 Model Validation 81
5.2.3 Parametric Study 85
5.3 EnergyPlus Modeling 91
5.3.1 Model Validation 91
5.3.2 Energy Savings of Proposed System 94
6. Conclusions 97
7. Future Work 98
References 100

List of Tables

Table 1: Summary of literature reviewed for vertical stratification measurement 13

Table 2: CFD research summaries – tall spaces, stratification, and heating season ... 20

Table 3: Size functions 27

Table 4: Solver settings 29

Table 5: Temperature profile discretization time slots 44

Table 6: Number of lighting fixtures in each room 49

Table 7: Thermal properties of concrete floor 51

Table 8: Roof construction thermal properties 52

Table 9: Fan Static Pressure Drop (McQuiston et al., 2004) 58

Table 10: Total Pressure Loss in Ducts 59

Table 11: EnergyPlus Fan Object Inputs 59

Table 12: Rooftop unit specifications before and after retrofit 63

Table 13: Air compressor model status 65

Table 14: Monthly electricity and gas consumption before and after retrofits 71

Table 15: Yearly energy savings of switching from metal halide to LED bulbs 74

Table 16: RTU retrofit energy savings 74

Table 17: Electricity savings due to XChanger calculated from utility bills 75

Table 18: Facility gas consumption before and after retrofits 77

Table 19: Grid sensitivity number of cells 80

Table 20: Parametric study test matrix 85

Table 21: Parametric study results (averages over entire flow domain)..... 87

Table 22: Average temperature minus hypothetical thermostat temperature 88

Table 23: Parametric study results; averages over the occupied zone..... 89

Table 24: ASHRAE guideline 14 requirements..... 91

Table 25: 2015 EnergyPlus model calibration statistics 91

Table 26: Temperature profile corresponding to model and time period 94

Table 27: Models used to compare fan controls and static pressure rise..... 95

Table 28: Energy savings of XChanger based on EnergyPlus models 96

List of Figures

Figure 1: Overhead Air Delivery (source: Bettinger West) 3

Figure 2: Conventional system and new system in cooling and heating 5

Figure 3: XChanger box working mechanism (XChanger Co., 2016) 6

Figure 4: Test facility layout and pole location 8

Figure 5: Large manufacturing room with traditional air delivery 9

Figure 6: Assembly room thermal image (metal halide lights) 9

Figure 7: Lighting image: metal halide fixture (left) vs. LED fixture (right) 10

Figure 8: Mixing ventilation (left) and XChanger (right) 10

Figure 9: Floor-level air supply device by Singh and Olivieri (1988) 11

Figure 10: Temperature measurement pole 14

Figure 11: Procedure for generating a reliable CFD model 17

Figure 12: Large manufacturing room with XChanger 24

Figure 13: Chosen location for CFD simulation 25

Figure 14: CFD geometry 26

Figure 15: Mesh along the supply diffuser vertical plane 26

Figure 16: Y-star values for heat transfer surfaces 28

Figure 17: Temperature profile boundary condition for walls 31

Figure 18: Room temperature distribution modeling approaches 33

Figure 19: Non-dimensional height room air model 36

Figure 20: Heat balance calculation procedure for non-uniform air temperature 37

Figure 21: Proposed method of accounting for thermostat offset 42
Figure 22: Input thermostat temperatures 43
Figure 23: Manufacturing electrical equipment schedule 46
Figure 24: Lighting schedule 47
Figure 25: Wall insulation properties (source: Masonry Advisory Council) 50
Figure 26: Built-up roof construction (source: Lydick-Hooks Roofing) 52
Figure 27: Typical air loop for a single space 53
Figure 28: Quadratic performance curves for the RTUs 55
Figure 29: Fan part load power as a function of flow fraction 60
Figure 30: Temperature profile measured during bay door opening 61
Figure 31: Air change rate due to infiltration 62
Figure 32: Map for thermocouple column naming 66
Figure 33: Average seasonal temperature of each thermocouple 67
Figure 34: Average measured temperature profile by room 68
Figure 35: Monthly degree day regression for (a) heating, (b) cooling 72
Figure 36: Degree day normalization for daily data 72
Figure 37: CDD increase from 2014 (baseline) to 2015 (post-retrofit) 73
Figure 38: Grid sensitivity – vertical temperature profiles 80
Figure 39: Measured supply air temperature of one RTU from 8/30/15 – 9/2/15 82
Figure 40: (a) Baseline and (b) XChanger CFD model validation 83
Figure 41: Vertical temperature profile measurement locations 84

Figure 42: (a) Baseline and (b) XChanger with the opposite boundary conditions.... 85

Figure 43: ASHRAE definition of occupied zone 89

Figure 44: PPD contours for each case (only high velocity cases shown) 90

Figure 45: Model versus measured daily electricity use..... 92

Figure 46: Accuracy of simulated daily electricity consumption 92

Figure 47: Simulated and measured monthly gas use..... 94

Nomenclature

Abbreviations

CNC	Computer Numerical Control
COP	Coefficient of Performance
DV	Displacement Ventilation
GFRC	Glass Fiber Reinforced Concrete
MAT	Mean Air Temperature
RANS	Reynolds Averaged Navier Stokes
RAT	Return Air Temperature
RTU	Roof Top Unit
UFAD	Under Floor Air Distribution
VAV	Variable Air Volume

Symbols

amb	Ambient (Outdoor)
I_{design}	Design Infiltration (m^3/s)
$F_{schedule}$	Scheduled Fraction
v	Velocity
$\dot{Q}$	Capacity (W)
Q	Heat (J)
$\dot{V}$	Volume flow rate (m^3/s)

1. Introduction

1.1 Motivation

Commercial buildings accounted for 18% of the total U.S. energy consumption in 2014 (EIA, 2015). Of this energy consumption, space heating constitutes 22.5% and space cooling constitutes 14.8%. From 2003 to 2012, the number of commercial buildings increased by 14% and the floor space of commercial buildings increased by 21%. An increase in the number and size of commercial buildings calls for more efficient building energy use. Numerous strategies exist for conserving building HVAC energy, such as more efficient primary systems, controls, and improvements to the building envelope.

Control over indoor air distribution is another possible way to save HVAC energy. Air distribution has been researched for roughly the past 35 years, focusing particularly on underfloor air distribution (UFAD) and displacement ventilation (DV). These strategies utilize low velocity supply air diffusers near the floor to provide cooling to the occupied zone. Although large differences between simulated and measured energy savings are reported in the literature, some researchers claim that UFAD saves 30% cooling energy, particularly in spaces with tall ceilings (Alajmi et al., 2010). However, these air distribution strategies do not lend themselves easily to the retrofit of existing buildings because they require different supply air

temperatures and velocities than traditional, packaged heating and cooling systems are designed to provide.

UFAD and DV raise an interesting question: how can thermal stratification be utilized to influence thermal comfort, indoor air quality, and the room's heating or cooling load?

1.2 Conventional Air Delivery Strategy for High Bay Buildings

Typical high bay buildings, such as warehouses, storage facilities, or hangars, use packaged rooftop units (RTUs) to condition indoor air. Due to high ceilings, often over 6 m, strong thermal stratification can develop because the density of air decreases as temperature increases. Cold, dense air accumulates near the floor, while warmer air floats towards the ceiling. This stratification has implications on building energy use and occupant thermal comfort.

Air is typically supplied and returned at ceiling level. This type of system will henceforth be known as the conventional or overhead system. The corresponding room air distribution strategy is called mixing ventilation. Air is often supplied horizontally using a wall duct, terminal device, or conical diffuser. An introduction to the design and behavior of the overhead system can be found in *Heating, Ventilating, and Air Conditioning* (McQuiston, 2004). When high velocity air is supplied horizontally near the ceiling, the jet of supply air attaches to the ceiling (the coanda effect), which increases its throw. As the jet flows along the ceiling, room air is

entrained and the jet decreases velocity to less than about 0.25 m/s. The jet is eventually fully mixed with the room air.

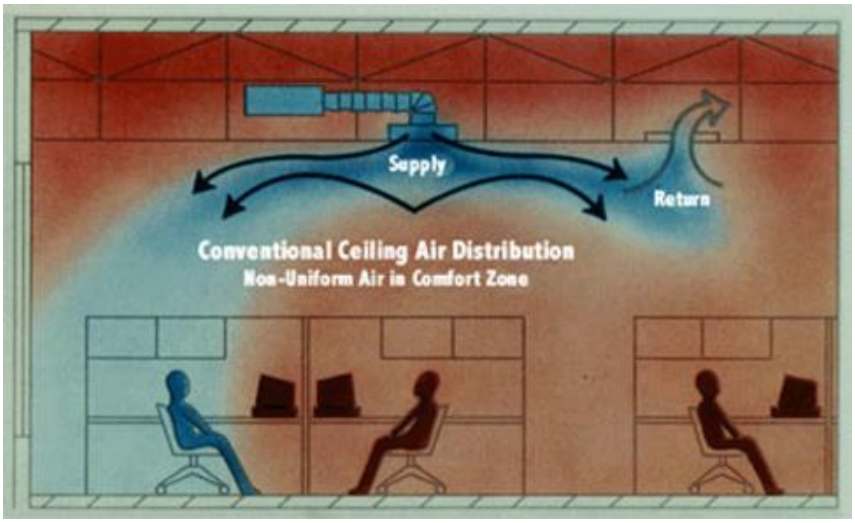

Figure 1: Overhead Air Delivery (source: Bettinger West)

McQuiston et al. point out that the conventional system is popular in commercial applications because "the ceiling diffuser can handle larger quantities of air at higher velocities than most other types" (McQuiston et al., 2004). With regards to creating a uniform temperature in the space, the authors concluded that "the ceiling diffuser is quite effective for cooling applications but generally poor for heating".

One problem with the traditional design is that the ceiling-level return duct draws the warmest air in the space. McQuiston described that "in spaces with very high ceilings, atriums, sky-lights, or large vertical glass surfaces and where the highest areas are not occupied, air stratification is a desirable energy-saving technique and return grilles should not be located in those areas [near the ceiling]".

Another problem with the conventional system occurs when supply air flows into the return duct before fully mixing with the room air. This short circuiting of supply air can be seen in Figure 1. Short circuiting is a waste of energy because the fans and cooling coil must operate longer to satisfy the space load.

1.3 Proposed Air Delivery System

A new air delivery system has been proposed by a Maryland based company to fix the two problems discussed above - returning the warmest air in the space and short circuiting the supply air (XChanger Co., 2016). This system reconfigures the location of supply and return ducts with the goal of saving energy and improving thermal comfort. With regard to published literature, this system can be thought of as a hybrid between the conventional, overhead system and UFAD or DV. It is a hybrid in that the system is simply a retrofit of the overhead system's ducting to produce a vertical temperature gradient that can be found in UFAD or DV systems.

In cooling season, air is supplied low and returned at a middle level. The goal is to condition only the occupied space. Of course, heat will still be transferred from the upper portion to the lower portion of the space by convection and radiation. However, the average temperature of the space will increase, which decreases the heat loss through conduction to the outside.

In winter, air is supplied near the ceiling and the return duct is located in the occupied zone. This configuration draws the warm air downward, thus destratifying

the space. Destratification reduces over-heating of the upper portion of the space and makes for easier-to-reach set points.

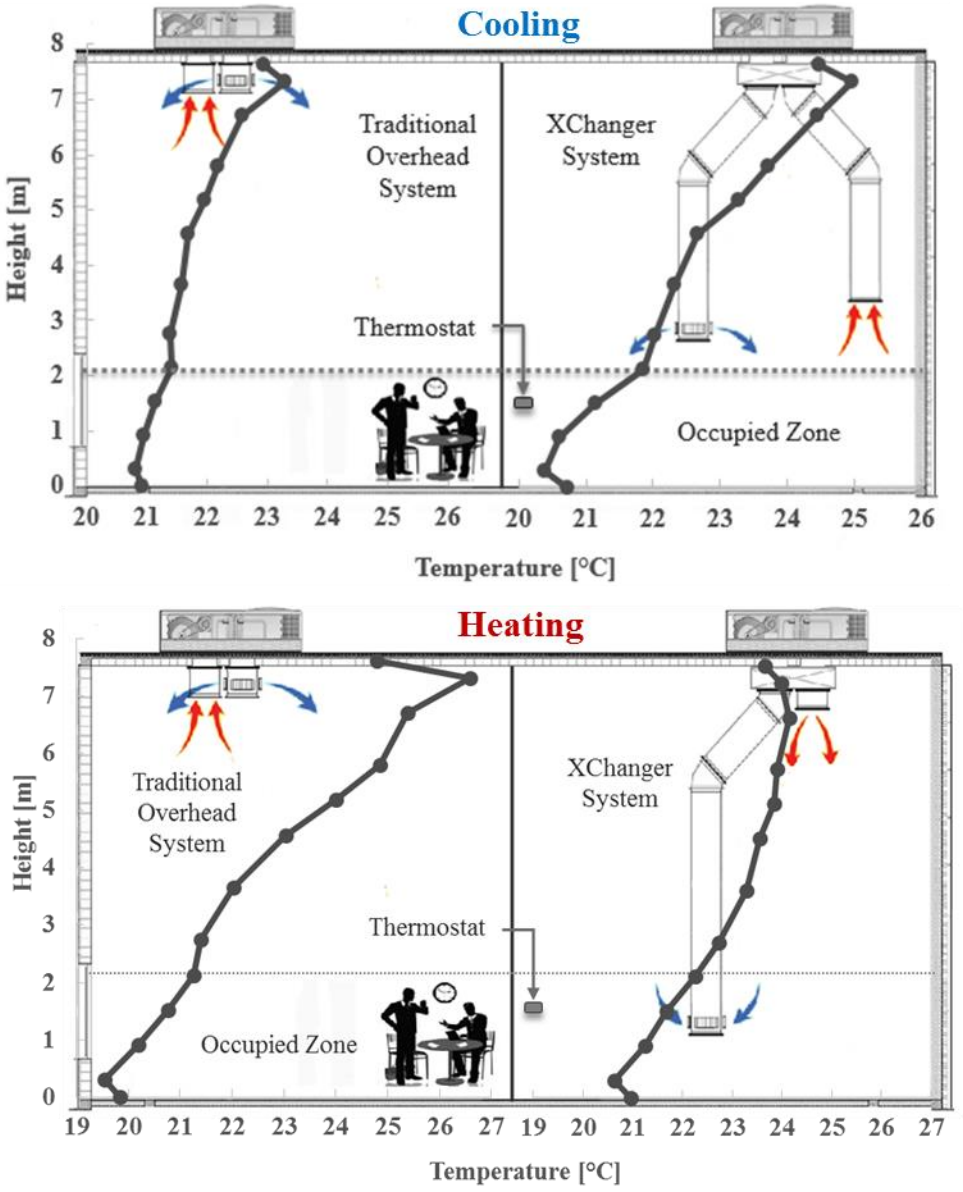

Figure 2: Conventional system and new system in cooling and heating

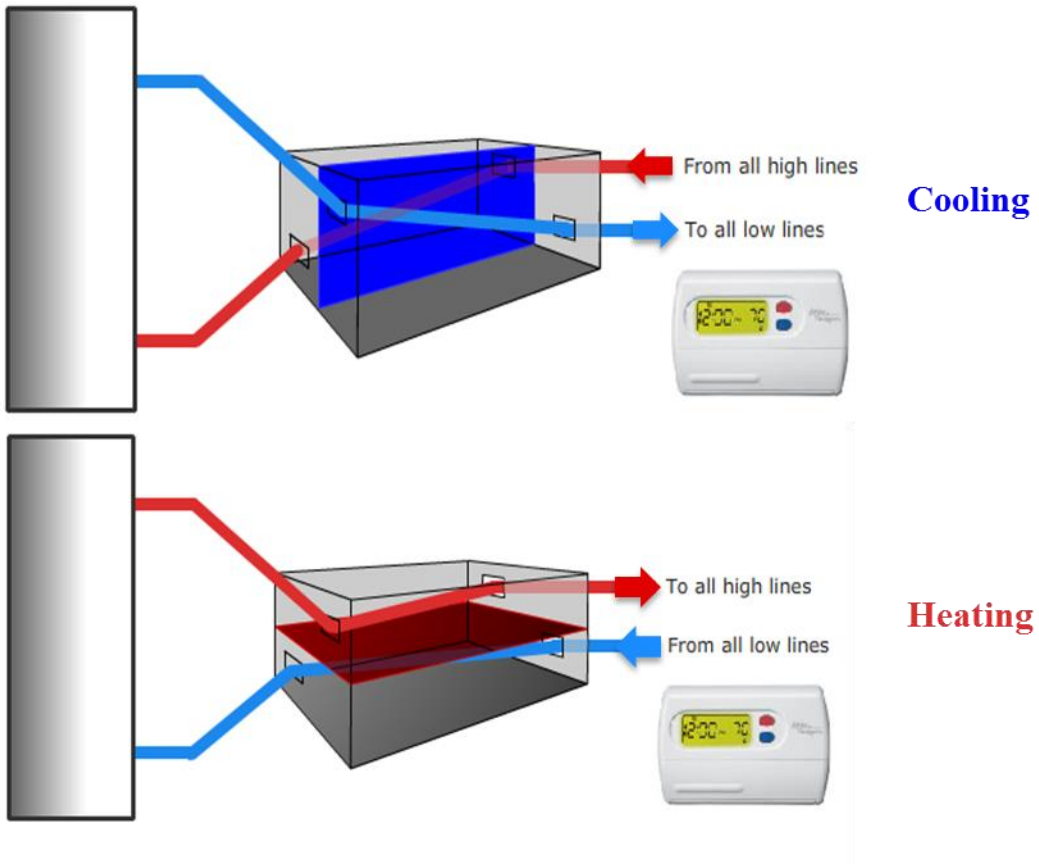

Figure 3: XChanger box working mechanism (XChanger Co., 2016)

The XChanger system is incorporated into a building with fixed ductwork as a retrofit or into a new building. During a retrofit, the existing ductwork is extended to the floor where convenient. To switch from supplying low, returning high in the summer to supplying high, returning low in the winter, the XChanger system has a 'box' with a single damper, as shown in Figure 3.

1.4 Objective

It is currently unknown how much energy the XChanger system will save a typical building. The objective of this thesis is to determine the energy savings associated with stratification in high bay buildings through experiment and modeling.

2. Experimental Work

2.1 Test Facility

Holmatro, a manufacturer of hydraulic rescue equipment from Glenn Burnie, Maryland, has installed four energy conserving retrofits: LED lighting, higher SEER rooftop units, the XChanger system, and a more efficient industrial air compressor. Holmatro has allowed measurements to be taken at their test facility for over one year. The purpose of the measurements was to track the performance and energy savings of the XChanger system over the course of one year. The facility layout, large manufacturing room, assembly room, lighting retrofit, and the XChanger retrofit can be seen in Figure 4 through Figure 8.

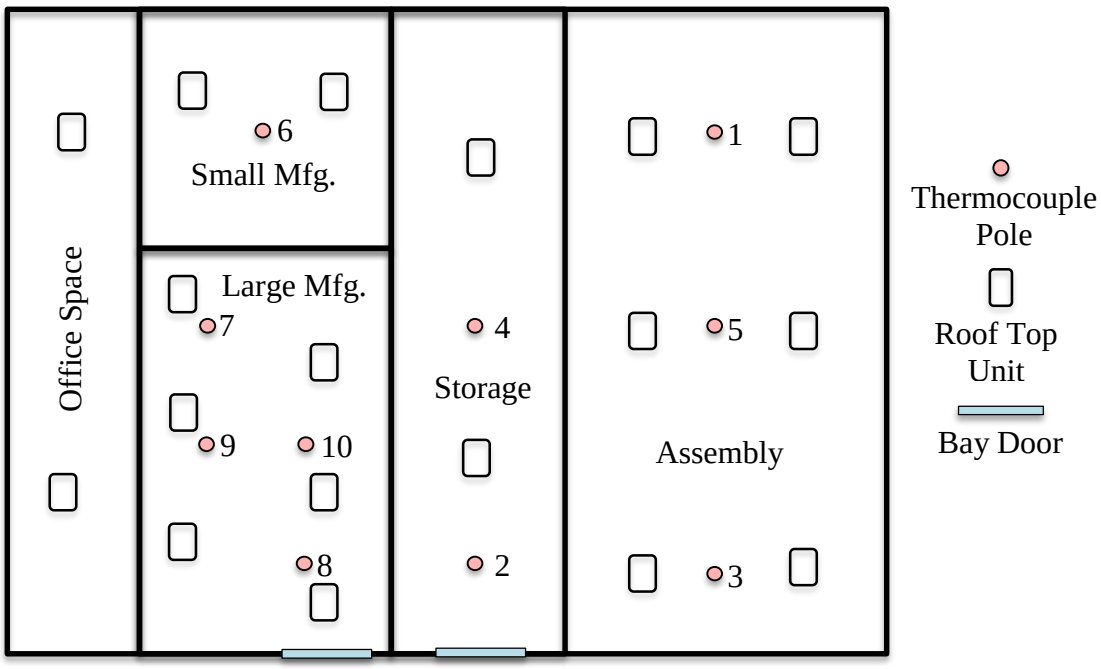

Figure 4: Test facility layout and pole location

The site consists of four large rooms and several offices. The offices take up two floors and have a central hallway running through the middle. The south side of the building has two large bay doors that open roughly twice per day for a few minutes to load and unload deliveries.

Figure 5: Large manufacturing room with traditional air delivery

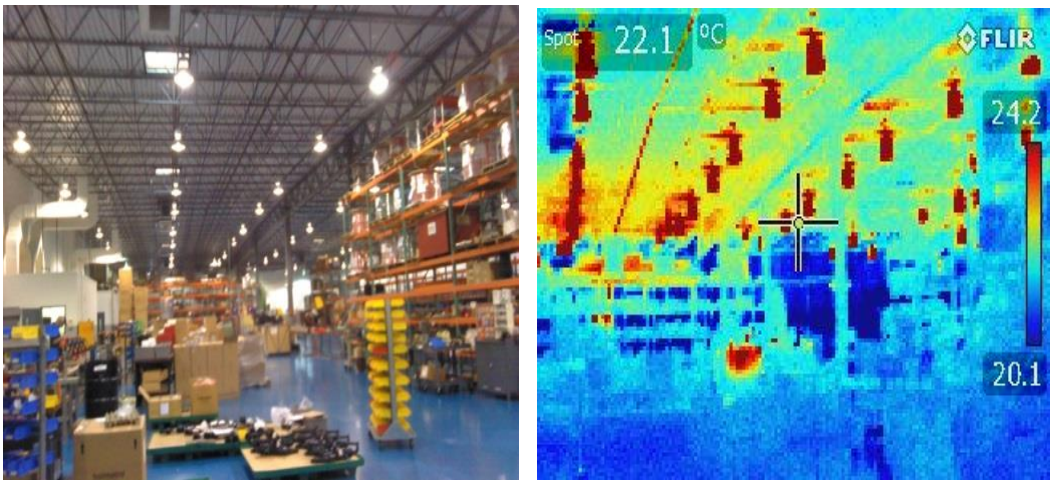

Figure 6: Assembly room thermal image (metal halide lights)

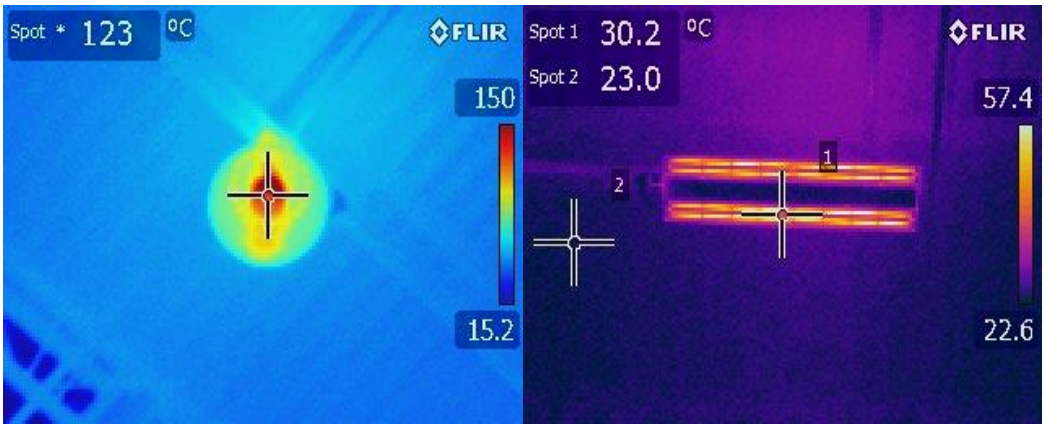

Figure 7: Lighting image: metal halide fixture (left) vs. LED fixture (right)

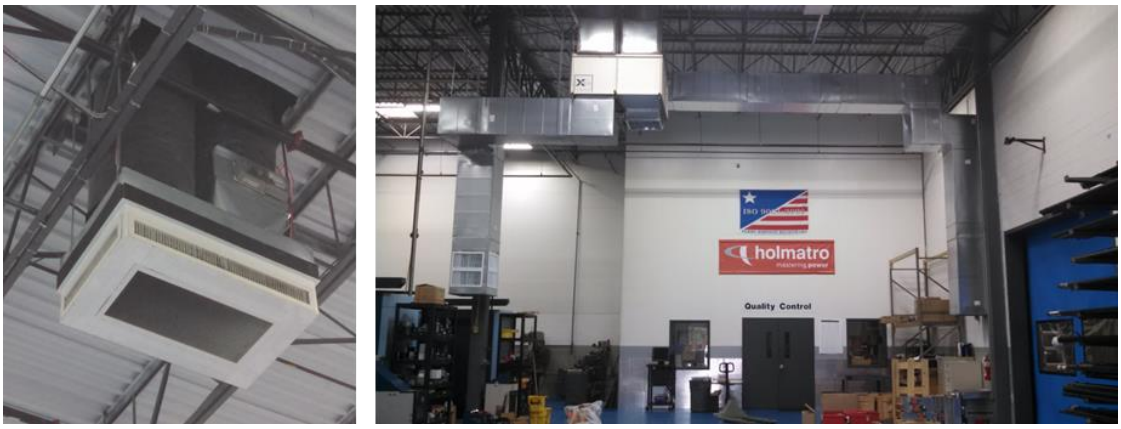

Figure 8: Mixing ventilation (left) and XChanger (right)

2.2 Literature Review

Researchers have used full-scale experiments to measure air distribution in buildings, particularly with UFAD, DV, and heating high-bay buildings. Singh and Olivieri tested a system very similar to the XChanger system that supplies and returns air near the floor (1988). Their idea to change the supply and return duct location stems from a desire to "eliminate either the effect of the induction of the upper level hot air into the supply air stream or the pulling down of the upper level hot air by the

return air or both". Through a series of ten tests, they reduced the height of supply and return ducts from ceiling-level to floor-level. The authors showed that supplying air in the bottom third of the room gives the most stratification and lowest occupied zone temperature. The return duct height has little effect on stratification, though they do not test low-level supply and high-level return.

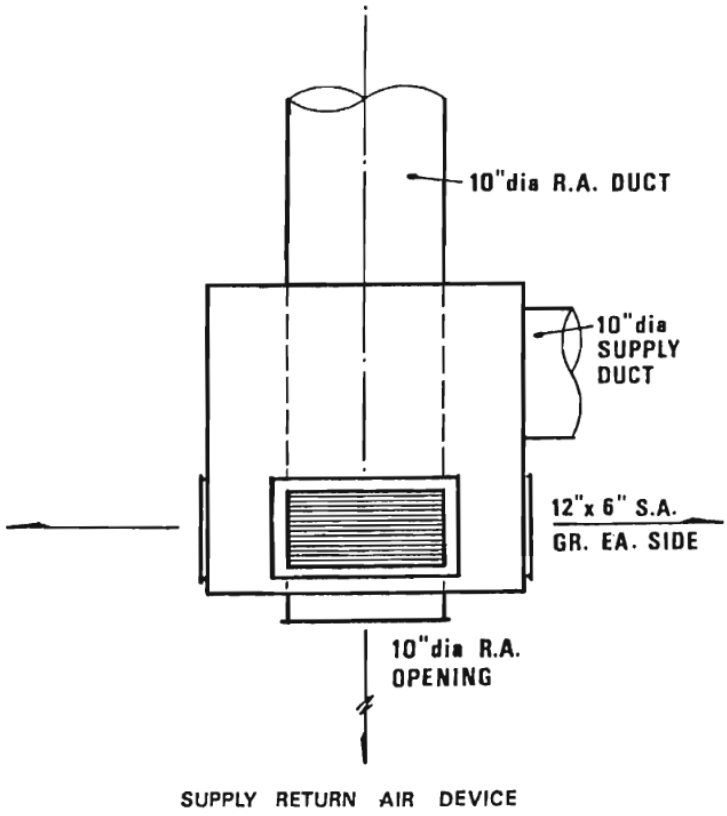

Figure 9: Floor-level air supply device by Singh and Olivieri (1988)

Using the device shown in Figure 9, the authors showed that a room with this device installed saves 33-50% RTU input power compared to a baseline room with a "four sided box with grilles on each face and central return air". The device in Figure

9 clearly resembles the XChanger and the air delivery ‘box’ that served as a baseline clearly resembles the overhead system in Figure 5. Based on this research, the XChanger system can be expected to save 33-50% HVAC energy in cooling, though the taller ceiling height in this thesis may affect the results.

Saïd et al. (1995) studied the effects of thermal stratification in large aircraft hangars during heating season. The heating system was the overhead down-draft air delivery system. Sixteen T-type thermocouples measure temperature from six inches off the floor to six inches from the ceiling. Temperatures were averaged over long measurement periods, giving stratification ranging from 4 K to 11 K. Two distinct, linear gradients are observed – one below 2 m and one above. Outdoor temperature and ceiling fans are shown to have little effect on stratification. No energy savings are reported from the experiment. BLAST simulations estimate a 38% reduction in gas use with no stratification compared to 8 K stratification.

Wang et al. (2011) studied an UFAD system in an 8 m tall gym. They conclude that supply air temperature influences the temperature gradient in the occupied zone, airflow distribution influences the temperature gradient in the middle of the room, and outside temperature has no influence on stratification.

Table 1: Summary of literature reviewed for vertical stratification measurement

Paper	Year	HVAC System	Ceiling Height [m]	Stratification [K]
Singh and Olivieri	1988	RTU with supply and returns at various heights	3.2 5.3	2.4 – 8.8 1.31
Said et al.	1995	Overhead heating	9.35 - 17.1	4 - 11
Wang et al.	2011	UFAD	8.0	7 - 19

2.3 Instrumentations and Data Acquisition

Ten vertical temperature poles were placed in the test facility, as shown in Figure 4. Each pole contains 13 thermocouples: one taped to the floor, one taped to the ceiling, and 11 measuring air temperature. Aluminum tape was used to attach the thermocouples to the floor and ceiling, insulating the thermocouple from air so that it accurately measured surface temperature. The vertical temperature poles were fastened to structural columns to avoid cluttering the shop floor and for access to an electrical outlet. A local wireless network was installed for communication between each DAQ board and a centrally located desktop computer. A mobile hotspot was used for remote Internet access to this desktop computer. Temperatures were measured over the course of one year, sampled every 20 seconds. Unfortunately, the wireless network breaks down periodically and measurements must be restarted manually.

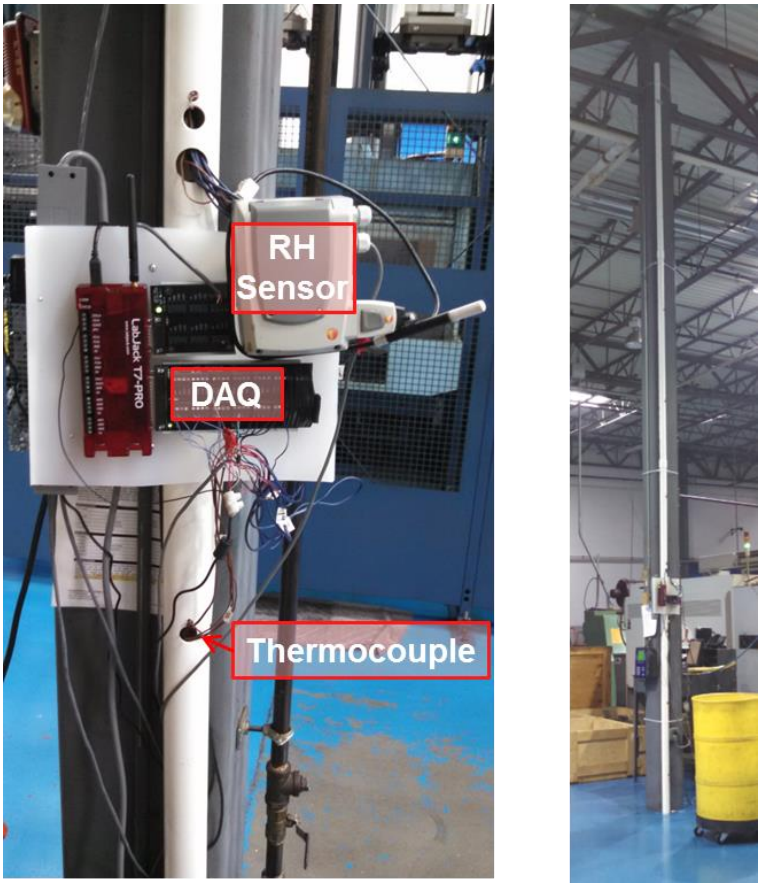

Figure 10: Temperature measurement pole

Seven relative humidity (RH) sensors were installed with at least one in every room. A one-time vertical RH profile was measured during cooling season to identify a potential humidity gradient. No such gradient was found, unless it is less than the measurement resolution of the sensors.

Five additional temperature measurements were made. One thermocouple from the large manufacturing room was extended to a supply duct to measure supply air temperature. Four wifi-enabled data loggers measured temperature and humidity of one RTU at four locations: inside the duct near the ceiling (directly from the RTU),

supply duct grille (outlet into room), inside the return duct near the ceiling (directly to the RTU), and return duct grille. The data loggers were used to measure heat loss along the XChanger ducting.

A watt-hour meter measured electricity consumption of one electrical panel that contains every RTU, except one, in the rooms that received the XChanger retrofit. This meter was used to estimate the HVAC energy use during the utility bill analysis.

2.4 Uncertainty Analysis

All thermocouples were permanently wired to their respective DAQ boards and calibrated in a temperature controlled water-glycol bath. The T-type thermocouples have an uncertainty of 0.5 °C. The RH sensors were 2% accurate. The watt-hour meter is 0.5% accurate.

3. Computational Fluid Dynamics Modeling

3.1 Literature Review

The use of computational Fluid Dynamics (CFD) modeling as a tool to study the indoor environment dates back to Nielsen in the 1970s (Jones and Whittle, 1992). Advances in CFD such as the Reynolds Averaged Navier Stokes (RANS) formulation, Launder and Spalding's k-ε turbulence model, and increased computational speed allowed more complex phenomena to be studied. By 1980, Gosman conducted a three-dimensional simulation using the k-ε turbulence model to study velocity distributions in rooms of various geometry.

Steady progress was made through the present, including the development of buoyant, low-Reynolds number models using the Boussinesq assumption (Chen, 1990), comparisons of various turbulence models for indoor flows (Chen, 1995; Zhang et al., 2007), development of methods to simulate supply diffusers (Srebric, 2000), and recommendations for obtaining boundary conditions from experimental data (Yuan et al., 1999; Chen and Srebric, 2002; Hajdukiewicz 2013).

Since CFD modeling has numerous potential pitfalls and subtleties, such as improper numerical techniques (discretization, precision, gradient evaluation), improper selection of boundary conditions (constant heat flux, constant temperature, radiation, turbulence), and improper use of models (wall treatment, turbulence modeling), there exists a need for a formal guide to utilizing CFD for the indoor

environment. *A Procedure for Verification, Validation, and Reporting of Indoor Environment CFD Analyses* by Chen and Srebric fills this role and is included in ASHRAE Fundamentals (2002). Verification is the identification of relevant physics and suitable CFD codes for a particular problem. Validation refers to the ability of a CFD code and user to reproduce experimental data through simulation. Reporting provides best-practice recommendations for how CFD users should report their work to ensure that it is complete and reproducible. This thesis will roughly follow the procedure laid out by Chen and Srebric for verification, validation, and reporting as well as the methodology provided by Hajdukiewics et al. (2013).

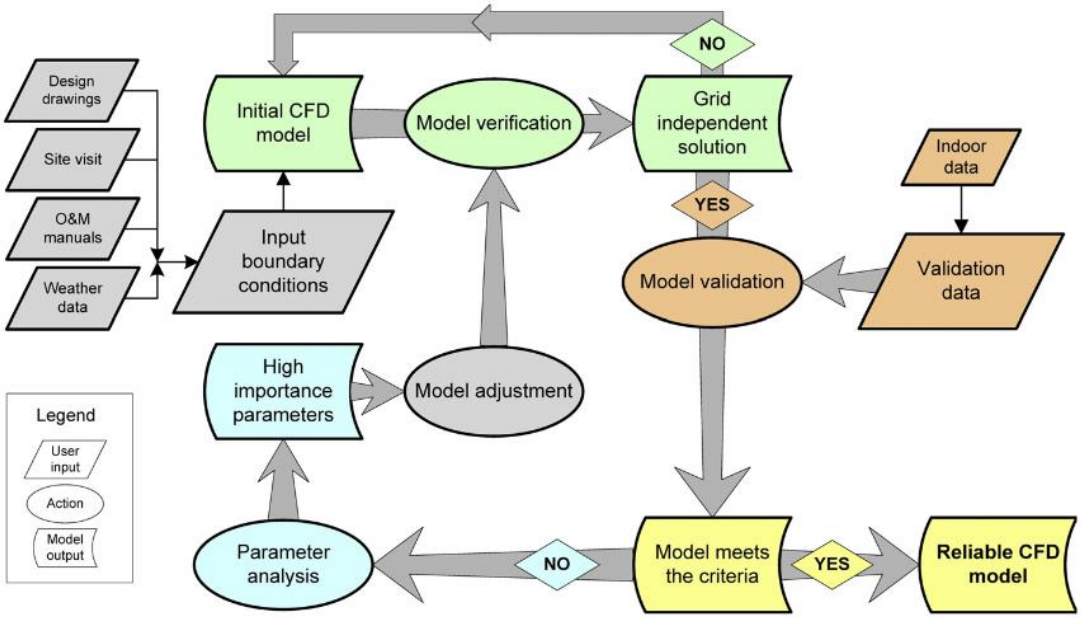

Figure 11: Procedure for generating a reliable CFD model (source: Hajdukiewicz et al., 2013)

Part of model verification is ensuring that the solution is independent of the computational grid used. More specifically, *grid convergence* is achieved when further refinement of a grid produces results that asymptotically approach some value, though not necessarily the experimental results (Roache, 1997). Model verification also requires that all relevant physics be simulated. The work presented in this thesis used ANSYS Fluent 15.0, which contains all modern CFD methods and techniques relevant to indoor environment flows.

Model validation refers to validation of both the model and the user as a pair. It was recommended by Chen and Zhai to 'work your way up' in complexity by simulating increasingly difficult flows and comparing the results to experiment (2004). Two of these flows were selected and attempted in order to gain confidence: two-dimensional natural convection with heated, vertical walls and a simple three-dimensional room with no flow obstacles. Although this exercise is easier than in 2004 due to increased computational speed, it was worthwhile to complete because it requires the CFD user to understand modeling techniques relevant to the indoor environment, like y+ values near walls, supply diffusers, and in cases with strong natural convection, oscillatory solutions.

Several papers have been reviewed that are relevant to this thesis due to their study of tall spaces with thermal stratification or relevant modeling techniques. Key items of interest have been noted, such as turbulence model, density-temperature coupling, and grid density. Although the required grid density is strongly dependent

on near-wall temperature gradient and velocity treatment, comparisons can be made for simulations with comparable physics and models (i.e. RANS indoor environment simulations with surfaces near room temperature).

Table 2: CFD research summaries – tall spaces, stratification, and heating season

Paper Title	Authors	Year	HVAC System Studied	Space Type	Model Details	Results and Conclusions
CFD simulation and evaluation of different heating systems installed in low energy building located in sub-arctic climate	Risberg, Vesterlund, Westerlund, Dahl	2015	Multiple	Home	• Sk-ε, scalable wall functions • Boussinesq • 7228 cells/m^3 • T_{supply} = 35-45 °C	• Convection-based heating systems lead to discomfort due to high air velocity • Emissivity and measured U-value for wall boundaries
CFD-simulation of indoor climate in low energy buildings computational setup	Risberg, Westerlund, Hellstrom	2015	Overhead heating	Two-room home	• Boussinesq • Sk-ε • 7500 cells/m^3	• As outdoor temperature increases, indoor stratification decreases due to smaller heat flux through wall
Indoor air environment and heat recovery ventilation in a passive school building: case study for winter condition	Wang, Kuckelkorn, Zhao, Mu, Spliethoff	2014	Heating, supply low, ceiling return	Classroom	• T_{supply} = 19 °C • 1795 cells/m^3	• Displacement ventilation at given supply temperature satisfies thermal comfort • Horizontal pollutant gradients
CFD simulation of temperature stratification for a building space: validation and sensitivity analysis	Gilani, Montazeri, Blocken	2013	Floor supply, ceiling return	Empty room with single heat source	• SST k-ω • 10852 cells/m^3 • $y^* < 1.8$ • ideal gas • UDF wall temperature	• Rk-ε model slightly outperforms others except k-ω • Grid resolutions using Roache GCI perform similarly
Stratified air distribution systems in a large lecture theatre: A numerical method to optimize thermal comfort and maximize energy saving	Cheng, Niu, Gao	2012	Floor supply, ceiling return	Theater	• RNG k-ε • 3758 cells/m^3 • Structured grid	• Ceiling exhaust with 8 °C stratification leads to cooling load reduction of 16.5% • Calculation method for energy savings

Cheng et al. (2012) simulated a stratified air distribution system in a five meter tall auditorium. An extensive parametric study was conducted where the supply location was changed from floor level in front of the occupants, floor level behind the occupants, and at desk level. This particular building featured separate return and exhaust ducts. This configuration allows the hottest air in the space to simply be exhausted, while the return is slightly cooler. The results showed that the cooling coil load is reduced by 12.3 - 16.5% depending on the supply configuration. The energy savings are explained to come from two sources: only the cooling load in the occupied zone needs to be met (accounting for radiation from the upper zone) and the splitting of return and exhaust ducts.

Very few simulations regarding heating can be found in the literature. The few papers that were found are summarized in Table 2 and have to do mostly with heat pumps (low supply temperature). The single exception involves an air heating system with supply air temperatures in the range of 40-50 °C, the temperature range of most gas heating systems. Unfortunately, only one paper provides model comparison with experimental data and its prediction was poor - within 1.2 °C.

3.2 Objective

CFD modeling is used in this work to study the effect of XChanger geometry on the mean temperature and velocity fields within the space. Particularly, supply height, return height, and supply face area were studied. The goal was to understand the influence of each of these parameters on the space and to recommend a set of parameters as the best performing for cooling applications.

Supply air temperature and flow rate are critical design variables of an air delivery system. Although other air delivery strategies, such as UFAD or displacement ventilation, may use

different supply air conditions than the conventional system, the goal of this work is to investigate the XChanger performance for buildings conditioned by rooftop units. Since typical packaged rooftop units have fixed supply air temperatures and flow rates, the supply air conditions are not considered as design variables.

3.3 Governing Equations and Turbulence Modeling

A standard CFD software package, Fluent 15.0 with Gambit 2.4, was used. Standard assumptions were made as follows:

- Three-dimensional, incompressible flow
- Negligible viscous dissipation in the energy equation
- Boussinesq density-temperature coupling
- Log-law velocity profile near walls

Mass Conservation $$\nabla \cdot (\rho \boldsymbol{u}) = 0 \quad \textbf{(1)}$$

Momentum Conservation $$\frac{\delta \boldsymbol{u}}{\delta t} + (\boldsymbol{u} \cdot \nabla)\boldsymbol{u} = \boldsymbol{g} + \nu \nabla^2 \boldsymbol{u} \quad \textbf{(2)}$$

Energy Conservation $$\frac{\delta E}{\delta t} + \nabla \cdot \left(\boldsymbol{u} \left(E + \frac{p}{\rho} \right) \right) = \nabla \cdot (k \nabla T) \quad \textbf{(3)}$$

The Boussinesq model, (4), treats density as a constant, except in the buoyancy term in the momentum equation (Fluent, 2013).

Boussinesq Assumption $$\rho = \rho_0 (1 - \beta \Delta T) \quad \textbf{(4)}$$

The constant ρ_0 is called the reference density and only needs to be input when there are multiple fluids present. β is the coefficient of thermal expansion. It was assumed to be 0.00343 1/K for air at standard temperature and pressure. The Boussinesq assumption is valid when $\beta \Delta T \ll 1$, which

is true for indoor environment flows. ΔT is the temperature difference between the fluid and a reasonable reference temperature, like 293 K.

Indoor environment flows can be classified as low velocity, low Reynolds number (Re) flows with flow regimes that can span laminar to turbulent flow (Zhai et al., 2007). Numerous papers have been published that judge the relative strengths and applicability of turbulence models to indoor environment flows, such Chen, 1995; Zhai et al., 2007; and Rohdin and Moshfegh, 2011.

Reynolds averaged Navier-Stokes (RANS) models remain the most commonly used turbulence models due to their robustness, speed, and large set of validation studies in the literature. Of the RANS models, the k-ε model is most common. Of k-ε models, there exists the standard, renormalization group (RNG), and realizable models. The RNG model is the most common turbulence model for indoor environment flows and is generally the most accurate (Zhai et al., 2007). The realizable k-ε model usually produces improved results for swirling flows and separation flows. Shih et al. (1995) showed that the realizable model outperforms the RNG model for predicting buoyancy in plumes. The realizable and RNG models were both tested using the validated baseline CFD model in this study. The two models produced nearly identical results, but the RNG model predicted turbulent viscosity ratios far exceeding the software's default maximum value. Therefore, the realizable model was chosen with the Fluent 15.0 default coefficients as the turbulence model used in this work.

3.4 Geometry and Computational Grid

The influence of the XChanger system in the manufacturing rooms is of interest in this study because they have the largest cooling load. Therefore, the CFD efforts were geared towards these rooms. However, these rooms are too large to simulate with 1850 m^2 floorspace.

Additionally, these rooms are served by multiple RTUs which further complicates the simulation.

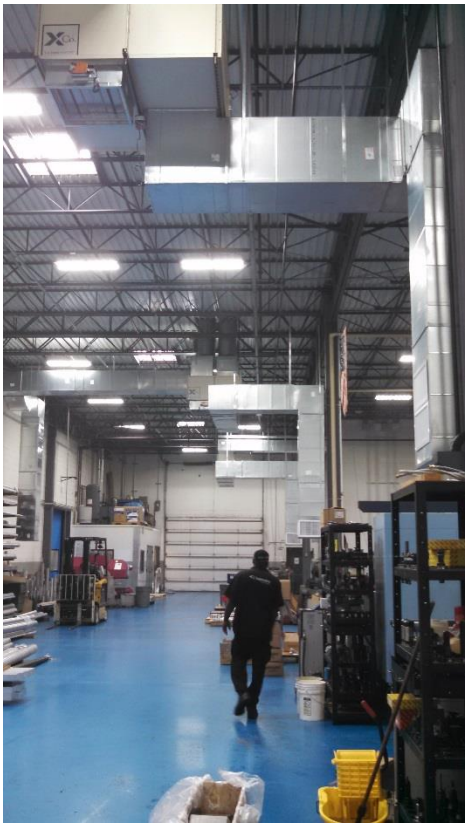

Figure 12: Large manufacturing room with XChanger

Since the large manufacturing room is too large to simulate and is served by six RTUs, one sixth of the room was simulated, as shown in the red box of Figure 13: Chosen location for CFD simulation. The boundary conditions for the 'invisible' walls is simply the measured temperature profiles of the air in the space. The red box in Figure 13 can be seen as the far back left corner of Figure 5. This geometry, RTU location, light location, and number of machines were roughly replicated in the CFD model.

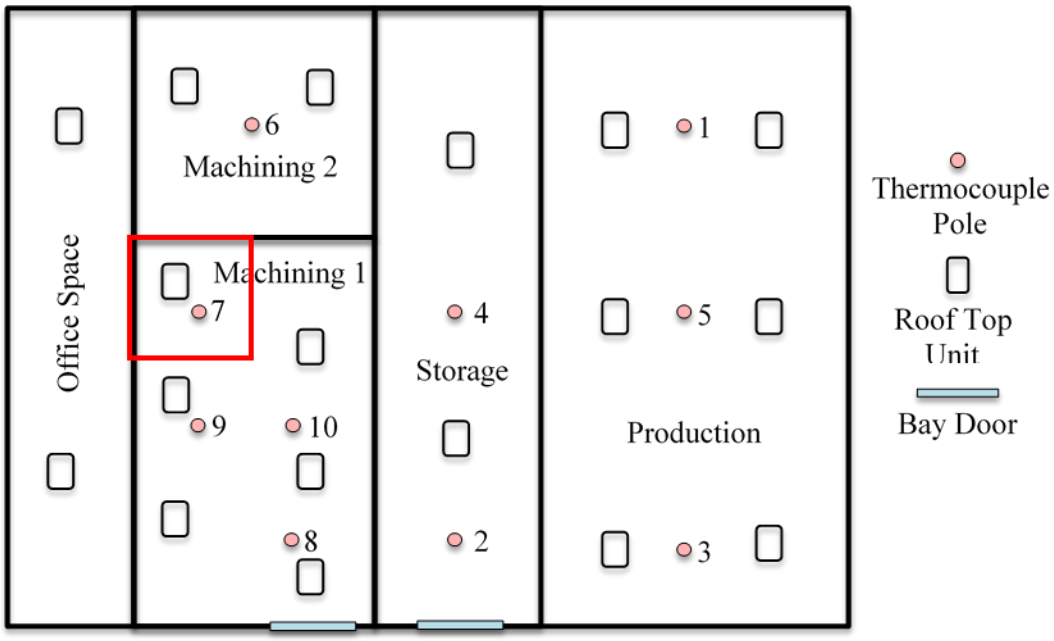

Figure 13: Chosen location for CFD simulation

The CFD model geometry is shown in Figure 14. The space is 9.1 m wide, 15.2 m long, and 7.62 m tall (30x50x25 ft) for a total volume of 1,054 m^3 (37500 ft^3). Since the model geometry only roughly replicates the real geometry, detailed surfaces are not necessary for the occupants and machines. This 'block' approach for simulating occupants has been shown to produce accurate mean air temperature and velocity fields sufficiently far from the occupant (Topp et al., 2002).

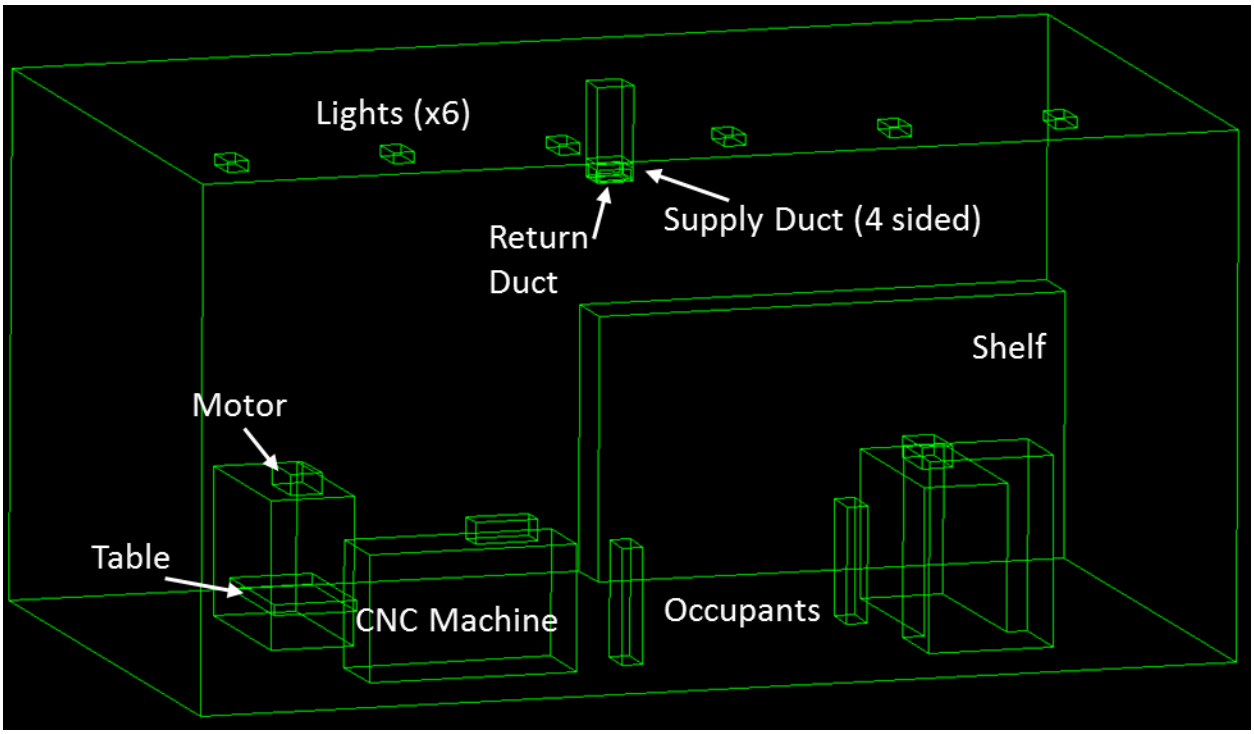

Figure 14: CFD geometry

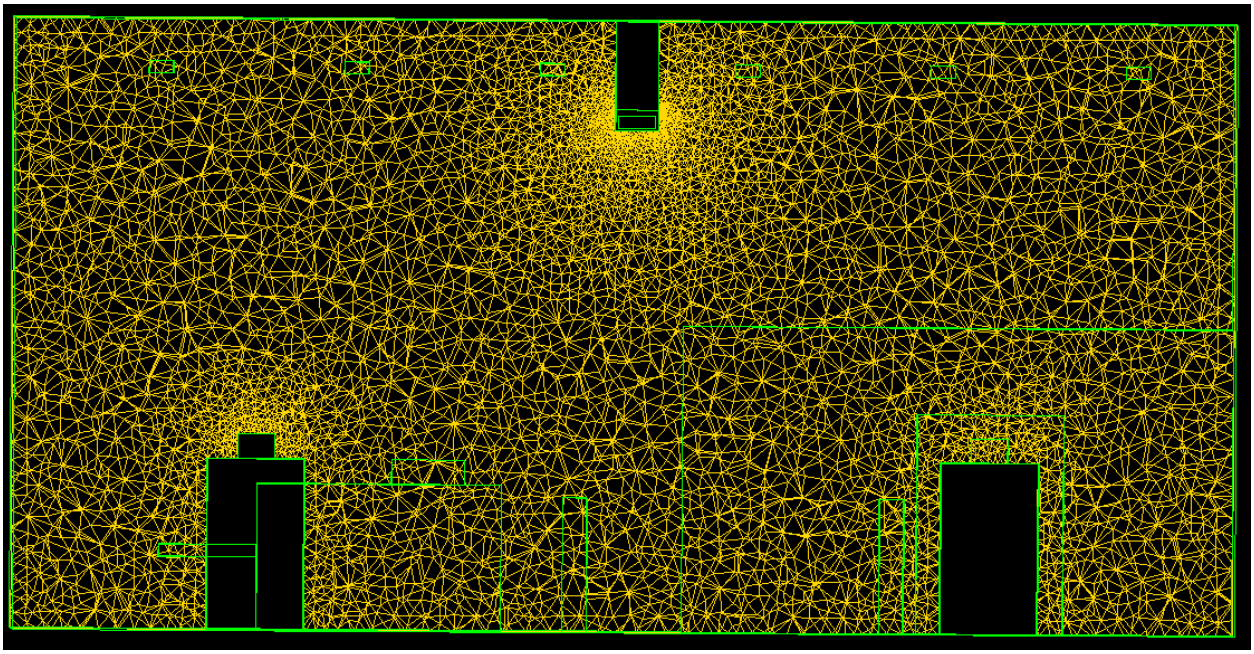

Figure 15: Mesh along the supply diffuser vertical plane

An unstructured mesh was used due to the decreased meshing time and effort required to produce a mesh with 'holes' in the domain (holes for the lights). Per the Fluent user guide, the

log-law for mean velocity near the wall is known to be valid when the dimensionless wall distance, y*, is between 30 and 300. Size functions were used iteratively with initial simulations to ensure y* values were less than 300. Several important size functions are summarized in the following table. The final mesh size was roughly 750,000 cells as determined by a grid sensitivity analysis. See the Results section for more information.

Table 3: Size functions

Object	Minimum Edge Length [m]	Growth Rate
Floor, wall, ceiling	0.23	1.4
Inlet	0.03	1.2
Outlet	0.06	1.2
Occupants / Machines	0.15	1.3
Lights	0.06	1.4

The y* values are typically below 300. For example, Figure 16 shows the y* values of the heat transfer surfaces. Only one cell is shown to have a y* value greater than 300. Notably, the lights have a y* value less than the recommended minimum, 11.25. Such a fine mesh was used here because the lights are small, yet it was desired to have at least two elements per edge. Since y* values can be below the recommended minimum for the log-law treatment, 'enhanced wall functions' were used. These ensure that the proper near-wall treatment, either the two-layer model or wall functions, is used based on a surface's y* value.

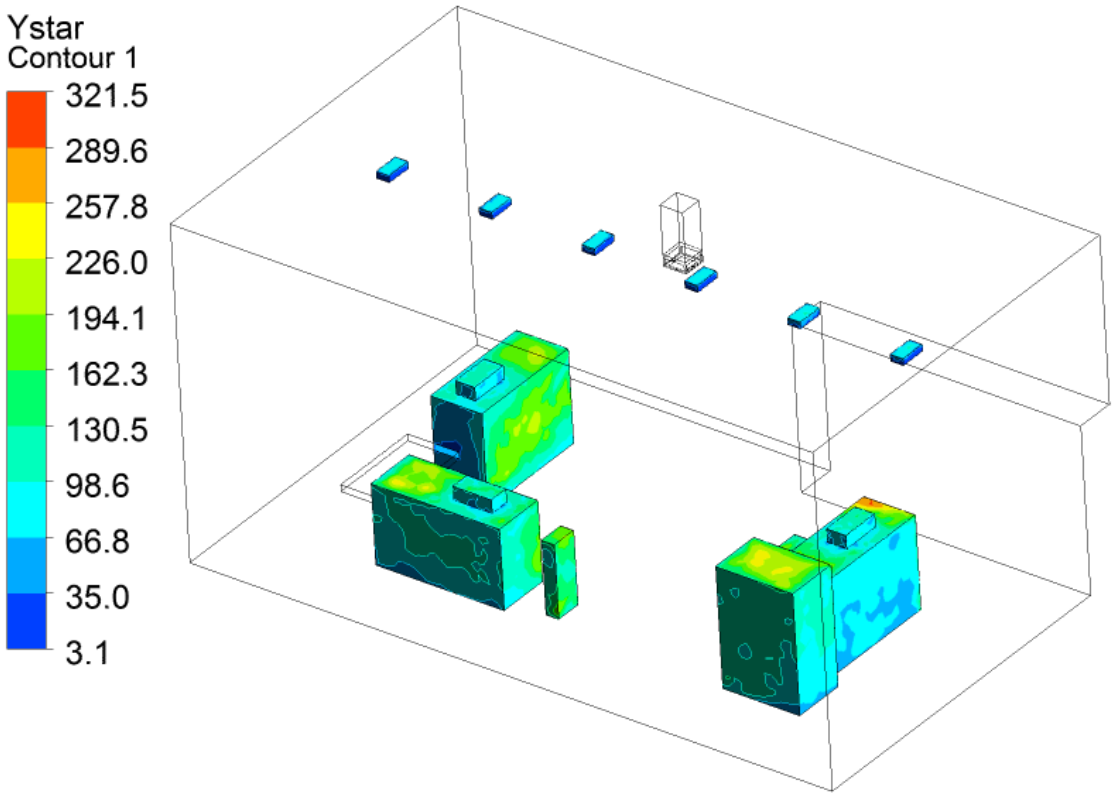

Figure 16: Y-star values for heat transfer surfaces

3.5 Solver Settings

Steady state temperature profiles were the main focus of this study. Therefore, the steady state solver should be used. However, it was difficult to achieve convergence of all residuals to less than 10^{-3}. It is believed that convergence in this thesis was difficult to achieve because of a coarse mesh (which is limited by computing resources). Therefore, the transient solver is used to simulate steady state phenomena. Convergence is judged by plotting two parameters: the overall heat transfer into the flow domain and vertical temperature profiles. The simulation runs until these parameters reach steady state – typically 20 to 30 minutes simulation time.

Table 4: Solver settings

Setting	Value	Rationale
Time	Transient	See above
Gravity	-9.81 m/s^2	
Density-temperature	Boussinesq	
Pressure-velocity coupling	PISO	Better for skew mesh
Gradient evaluation	Green-Gauss Node Based	Use with body force weighted pressure
Pressure discretization	Body Force Weighted	Better buoyancy prediction
Other discretizations	Second Order Upwind	Default

3.6 Boundary Conditions

The large manufacturing room has a large open doorway to the small manufacturing room, a bay door that opens about twice per day to the outside, and two large, automatic vinyl doors that separate it from the storage room. The machine load and occupancy vary throughout the day. Since it is difficult and unnecessary to take into account all of this phenomena to study stratification, 'representative' boundary conditions have been created. The goal was to simulate the same physics – forced and natural convection – that are present in the actual room.

Temperature measurements provided boundary conditions for the floor, wall, and ceiling. When a constant temperature boundary condition is specified, radiation becomes irrelevant to that surface. Since the floor, walls, and ceiling used constant temperature boundary conditions from the experiment and these surfaces made up most of the heat transfer area in the domain, radiation was neglected completely in the model. Further rationale for ignoring radiation came from the objective of this simulation – studying thermal stratification. If the focus were on heat transfer mechanisms within the space, radiation would be considered.

To simulate the occupants, a 'block' approach can be used, as in Top et al. (2002). They showed that a rectangular block has similar global influence to a detailed rendering of a human. A constant heat flux boundary condition was used for the surface of the occupants, 75 W/m^2, which produces 162.5 W per occupant. This value is typical of light, standing work.

The heat dissipation of CNC machines was difficult to know for several reasons. They operated at continuous part-load ratios, had internal air or water cooled heat exchangers, and stored heat due to their thermal mass. Therefore, they were assumed to have a constant surface temperature of 40 °C. The motors had a surface temperature of 66 °C.

The inlet boundary condition was a flat, rectangular face with constant velocity in the normal direction. The baseline unit has one duct that delivers air from the RTU to four orthogonal 0.15 x 0.46 m supply grilles. The actual RTUs in this room are rated for 2.6 m^3/s. Supply air temperature has been measured to be in the range of 8 °C to 20 °C. Since the RTUs cycle on and off and the supply temperature varies, it was difficult to assign a fixed value for the supply air flow rate based on the installed RTU. Therefore, an 'average' flow rate and temperature were used that produced results consistent with measurements. These values were found to be 0.56 m^3/s at 12 °C for the baseline simulation and 1.11 m^3/s at 14 °C for the XChanger simulation. Ideally, the same boundary conditions would be used for baseline and XChanger cases. This discrepancy is discussed further in Section 5.2.2. The outlet boundary condition is 'outflow' with zero pressure difference.

The temperature profiles specified vertically along the walls comes from the average thermocouple value during the summer. The value of the floor, ceiling, and wall temperature can be seen below. They were generated using a least-squares fit of the measured data and implemented using user-defined functions.

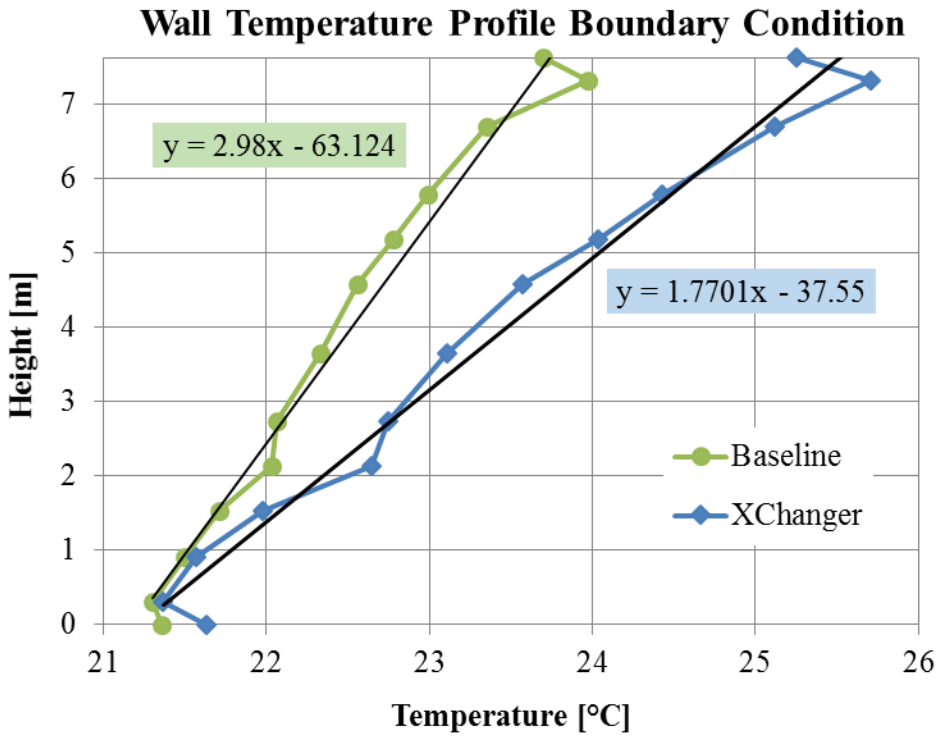

Figure 17: Temperature profile boundary condition for walls

4. Building Energy Simulation

4.1 Literature Review

Since its inception in the 1970s due in part to the energy crisis, building energy simulation has evolved from a simple load and sizing calculator to a well-established branch of building science. Modern building energy simulation software is capable of simulating the transient performance of a building, including conduction, convection, and radiative heat transfer, solar heat gain, lighting, shading, and advanced HVAC systems as well as performing basic economic and life cycle cost analyses.

Recent energy efficiency policies, like California's stringent Title 24 standards, and energy efficiency incentives, such as Leadership in Energy and Environmental Design (LEED) accreditation, bring the use of building energy modeling into the design process of new constructions and renovations as a low-cost design tool. Various software packages have emerged as a result, such as EnergyPlus and its predecessor DOE-2, as well as solutions using equation-based modeling in TRNSYS and Modelica. DOE-2 evolved from the original BLAST software and was the standard building energy modeling software in the U.S. for three decades. Funded by the Department of Energy (DOE) in the late 1990s, EnergyPlus was developed to include more advanced modeling capabilities using a modular software design that is intended to attract third party development. Equation-based modeling using software like TRNSYS and Modelica requires more expertise but can produce accurate results for building performance, particularly for advanced topics like control systems (Haugstetter, 2006).

The goal of building energy modeling in this thesis is to investigate the energy savings of the installed retrofits, including efficient lighting, new RTUs, a new air compressor, and the XChanger ducting system. EnergyPlus was chosen as the simulation software because it is capable of capturing the known effects of installed retrofits on the building, particularly the distribution of air temperature within each room.

Simulating the effects of vertical temperature gradients, called room-air modeling, has been implemented by researchers in many different ways. Room airflow has been incorporated by coupling CFD modeling and building energy simulation (Nielsen and Tryggvason, 1998; Srebric et al., 2000). Coupling CFD and building energy simulation is useful for the purpose of calculating heat transfer coefficients, return air conditions, and thermal comfort. It is noted that this method is too costly to implement for an hour-to-hour simulation, but has merit when conducted on a typical day in a season, such as a 'design day'.

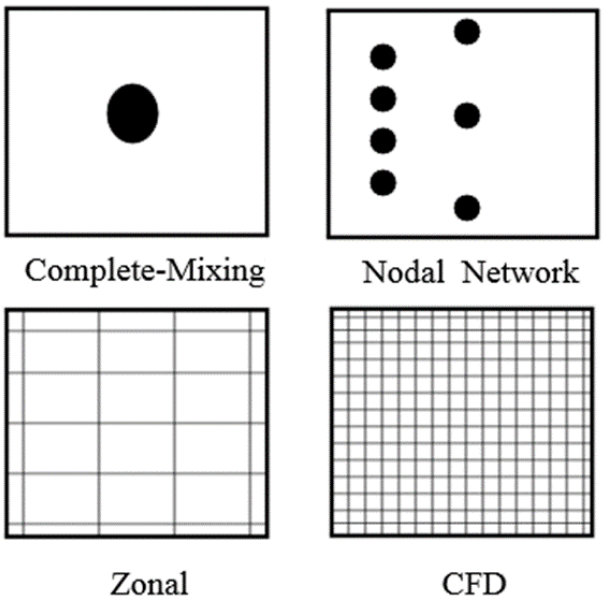

Figure 18: Room temperature distribution modeling approaches (source: Griffith, 2004)

Another method involves discretizing a space into zones, or small control volumes, and solving for mass and energy conservation among the zones (Griffith, and Chen 2003). These "zonal" models are able to predict air flow reasonably well, but increase computational time by two orders of magnitude. Zonal models are not currently included in commercially available software.

A third method of introducing room air flow into building energy simulations is called "nodal" modeling. Nodes are used to spatially prescribe a flow path, gradient, or property within a single zone. Nodal models require different inputs for each node depending on the application. Nodal models have been developed for sidewall displacement ventilation (Mundt, 1996), underfloor air distribution (UCSD models), and numerous discretizations of vertical temperature gradient, such as single-gradient, two-gradient, non-dimensional height, etc.

EnergyPlus has these nodal models available for use. For this thesis, the non-dimensional height model is chosen. For information regarding room-air models and the XChanger system, see Room Air Modeling. Uses of room air models in the literature are scarce.

Pan et al. (2010) used non-dimensional height room air models to simulate an 80-130 m tall atrium. They also have experimental measurements and CFD modeling. They found that the mixing model over-predicts the cooling load compared to the room-air model by 88-212%. The cooling load reduction by using the room air model was found to increase with the height of the space. It should be noted that this atrium had both a return duct and exhaust duct, whereas the test facility used in this thesis only has a return duct. Therefore, the discrepancy between mixing model and room-

air model will be lower. It was concluded that room-air modeling is necessary for tall spaces. However, no experimental validation was provided for the room-air models in that paper or any other paper found in the literature (with the exception of UFAD and DV).

4.2 Room Air Modeling

The goal of the present work is to estimate the energy savings due to different indoor vertical temperature profiles using EnergyPlus room-air modeling. The user-defined, non-dimensional height room air model was chosen because measured temperature profiles can be used directly. Additionally, inputs for return duct and thermostat temperatures are available.

Figure 19 shows one example of a non-dimensional height room air object. The vertical height is non-dimensionalized such that 0 represents the floor and 1 represents the ceiling. Temperatures are a function of height, where each height is called a node. At every node, the user inputs the difference between the node temperature and the room mean air temperature. The exhaust and return duct temperature offsets can be input as well. Although there exists an input for thermostat offset temperature, it is was found to not currently be used for anything other than reporting of an output variable *ZoneThermostatAirTemperature*. All node temperatures and offset temperatures float with the room's mean air temperature, as calculated in the EnergyPlus heat balance equations.

$$T(z) = T_{air,i} - T_{MAT}$$

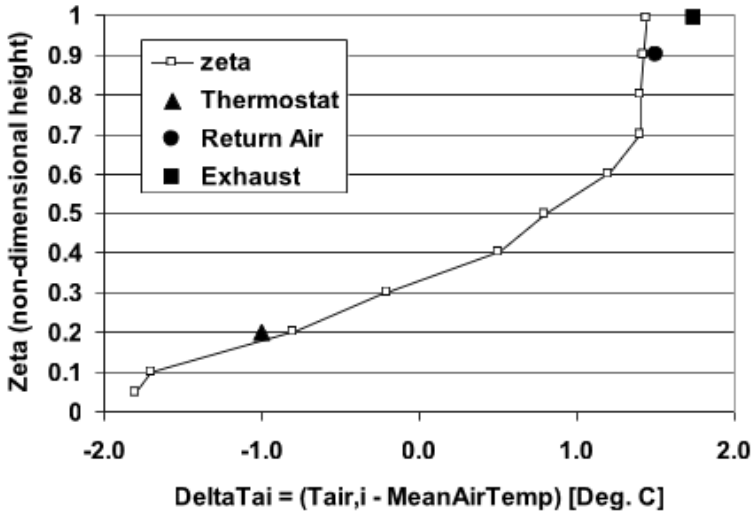

Figure 19: Non-dimensional height room air model (source: EnergyPlus IO manual)

The EnergyPlus non-dimensional height room air model is the result of a paper, *Framework for Coupling Room Air Models to Heat Balance Model Load and Energy Calculations* by Griffith and Chen in 2004. The authors alter the surface and air heat balance equations to incorporate non-uniform room air temperatures. A brief summary of their method is provided here.

EnergyPlus has two interacting loops: the air heat balance loop and the surface heat balance loop. These loops communicate each time step using a predictor-corrector approach to determine the thermal load of each zone. The addition of non-uniform room air temperatures requires the temperature from what was the fully-mixed model to now be implemented as a function of height. Figure 20 shows each heat transfer mechanism implemented with the non-dimensional height room air model in EnergyPlus.

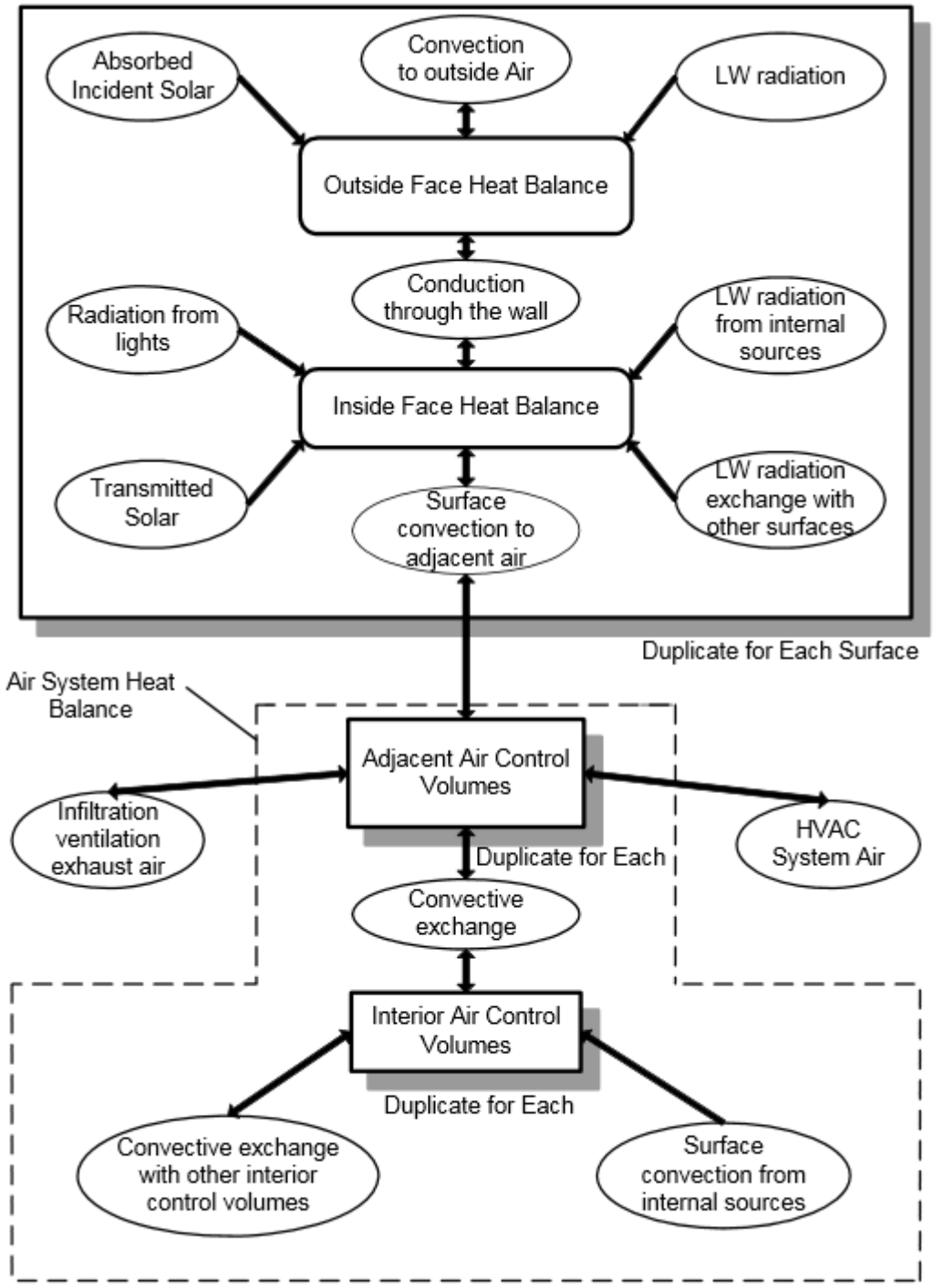

Figure 20: Heat balance calculation procedure for non-uniform room air temperature (source: Griffith and Chen, 2004)

While the outside face heat balance equations remain the same, the inside face heat balance equations must be rewritten to include vertical temperature profiles. Griffith and Chen (2004) altered the heat balance equations of Pedersen et al. (1997) to include subscripts *i* for vertical height. In (5), the surface heat balance equation, values for the convective heat transfer coefficients are obtained in the same manner as the well-mixed model – correlations. However, now each surface assumes $T_{a,i}$ is the associated reference temperature. Additionally, it is assumed that the reference temperature is assigned at a distance of roughly 0.1 m from the surface to ensure that it is "outside the inner thermal boundary layer but not too far outside".

$$T_{s_{i,j}} = \frac{T_{so_{i,j}} Y_{i,o} + \sum_{k=1}^{nz} T_{so_{i,j-k}} Y_{i,k} - \sum_{k=1}^{nz} T_{s_{i,j-k}} Z_{i,k} + \sum_{k=1}^{nq} \Phi_{i,k} q''_{ki_{i,j-k}} + T_{a_{i,j}} h_{c_{i,j}} + q''_{LWS} + q''_{LWX} + q''_{SW} + q''_{sol}}{Z_{i,o} + h_{c_{i,j}}} \quad \textbf{(5)}$$

where, T_s is the inside face temperature
i subscript indicates individual surfaces
j subscript indicates current time step
k subscript indicates time history steps
T_{so} is the outside face temperature
Y_i are the cross CTF coefficients
Z_i are the inside CTF coefficients
Φ_i are the flux CTF coefficients
q''_{ki} is the conduction heat flux through the surface
h_{c_i} is the surface convection heat transfer coefficient
T_a is the near-surface air temperature
q''_{LWS} is the long wave radiation heat flux from equipment in zone
q''_{LWX} is the net long wavelength radiation flux exchange between zone surfaces
q''_{SW} is the net short wavelength radiation flux to surface from lights
q''_{sol} is the absorbed direct and diffuse solar (short wavelength) radiation

Once the inside surface temperatures are found, they are passed to the air and surface heat balance, (6). This $\dot{Q}_{\text{sys}}$ value is then passed to the HVAC system loop.

$$\dot{Q}_{sys} = \sum_{i} A_i h_{c_i} \left(T_{s_{i,j}} - T_{a_{i,j}} \right) + \dot{Q}_{conv,S} + \dot{Q}_{Infil} \qquad \textbf{(6)}$$

Room air models have an input called 'coupling' which can be either direct or indirect. Indirect coupling uses "values for T_a from the air model as a relative distribution of differences [from set point temperature] and applies them to the control set point in the load/energy routines". With direct coupling, there is no notion of control. In other words:

$$\text{Indirect:} \quad T_{a_i} = T_{setpoint} + \Delta T_{a_i} \qquad \textbf{(7)}$$

$$\text{Direct:} \quad T_{a_i} = T_{MAT} + \Delta T_{a_i} \qquad \textbf{(8)}$$

The original paper that EnergyPlus documentation references includes both types of coupling. However, EnergyPlus currently only uses indirect coupling for the Mundt model. Therefore, the non-dimensional height room air object used in this thesis uses direct coupling and control based on room mean air temperature. Thermostat offset is implemented manually, as described later.

The return air temperature offset is coupled to the load calculation as follows. When computing the zone thermal load, the $\dot{Q}_{\text{sys}}$ value that has been previously computed is multiplied by a load correction factor *LCF*, (9), as shown in (10).

$$LCF = \frac{T_{supply} - T_{return}}{T_{supply} - T_{MAT}} \qquad \textbf{(9)}$$

$$\dot{Q}_{sys} = \dot{Q}_{sys,previous} * LCF \qquad \textbf{(10)}$$

The load correction factor is constrained to be between -3 and 3, though is typically close to unity.

The EnergyPlus heat balance routine iterates until convergence is met, meaning the zone mean air temperature minus the zone set point temperature is less than some tolerance, typically 0.4 ºC. In the original paper from Griffith and Chen described above, the air loop iterated until the air temperature *measured by the thermostat* minus zone set point temperature (the input) is within a tolerance. In other words, EnergyPlus controls the space such that the mean air temperature is the controlled variable, while in the original paper the space is controlled such that the air temperature measured by the thermostat is the controlled variable. The EnergyPlus Engineering Reference addresses this issue in the following way.

> "The room air models are coupled to the heat balance routines using the framework described by Griffith and Chen (2004). Their framework was modified to include features needed for a comprehensive program for annual energy modeling rather than one for hourly load calculations. The formulation is largely shifted from being based on the set point temperature to one based on the current mean air temperature. This is necessary to allow for floating temperatures and dual set point control where there may be times that the mean zone temperatures are inside the dead band."

The XChanger system has been shown to change the temperature profile of a space. For example, in summer the XChanger increased the difference between the temperature at the thermostat and the mean air temperature by 0.61°C in the large manufacturing room.

$$\text{Summer Baseline:} \quad T_{stat} - T_{MAT} = -0.71°C \qquad \textbf{(11)}$$

$$\text{XChanger:} \quad T_{stat} - T_{MAT} = -1.32°C \qquad \textbf{(12)}$$

However, this difference is not reflected in the EnergyPlus model because the model controls the space temperature based on its mean air temperature, not set point temperature. Therefore, a method has to be proposed to reflect the real thermostat.

The original implementation of room air models by Griffith and Chen would be relatively simple for an experienced EnergyPlus developer to implement. However, the complexity and sensitivity of the heat balance routines makes this task difficult for an inexperienced developer. Additionally, special care must be taken to ensure existence and uniqueness of solutions to the altered heat balance equations, as in Zhai and Chen (2003). Therefore, a simpler approach is proposed that does not involve altering the EnergyPlus source code.

Figure 21 shows the original room air model in EnergyPlus on the left and the desired model on the right. Using Griffith and Chen's notation, define:

$T_{setpoint}$	Input set point temperature
T_{stat}	Temperature measured by the thermostat

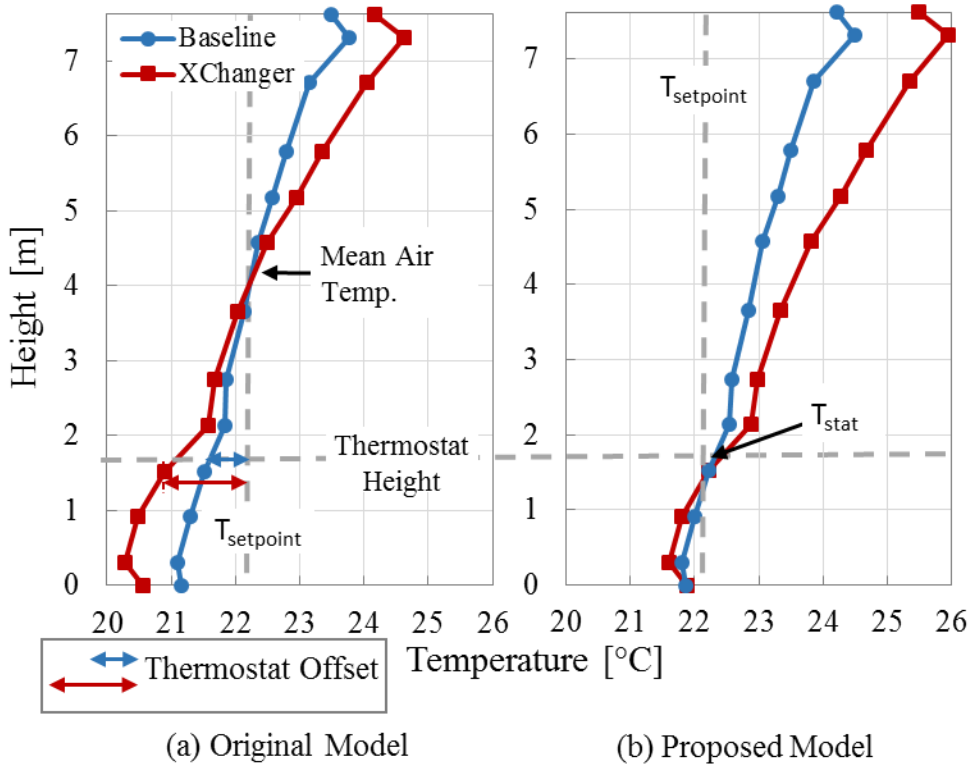

Figure 21: Proposed method of accounting for thermostat offset

The original model's heat balance equations act on the zone's mean air temperature, which is why the mean air temperature is equal to $T_{setpoint}$ for the original model. The actual time-averaged measured data is in figure (b). To modify the baseline model to produce the measured data, the set point of the zone must be increased by the amount given by the 'Thermostat Offset' arrows. For this example, the XChanger thermostat offset was 1.31°C and the baseline thermostat offset was 0.71°C. So, the thermostat model input, $T_{setpoint}$, was changed from 22.2°C (the test-facility's set point) to 23.53°C (22.2+1.31) for the XChanger model and 22.93°C (22.2+0.71) for the baseline model. Using this method, EnergyPlus will control the zone to its actual set

point, 22.2°C, as if there were a real thermostat sensing the temperature.

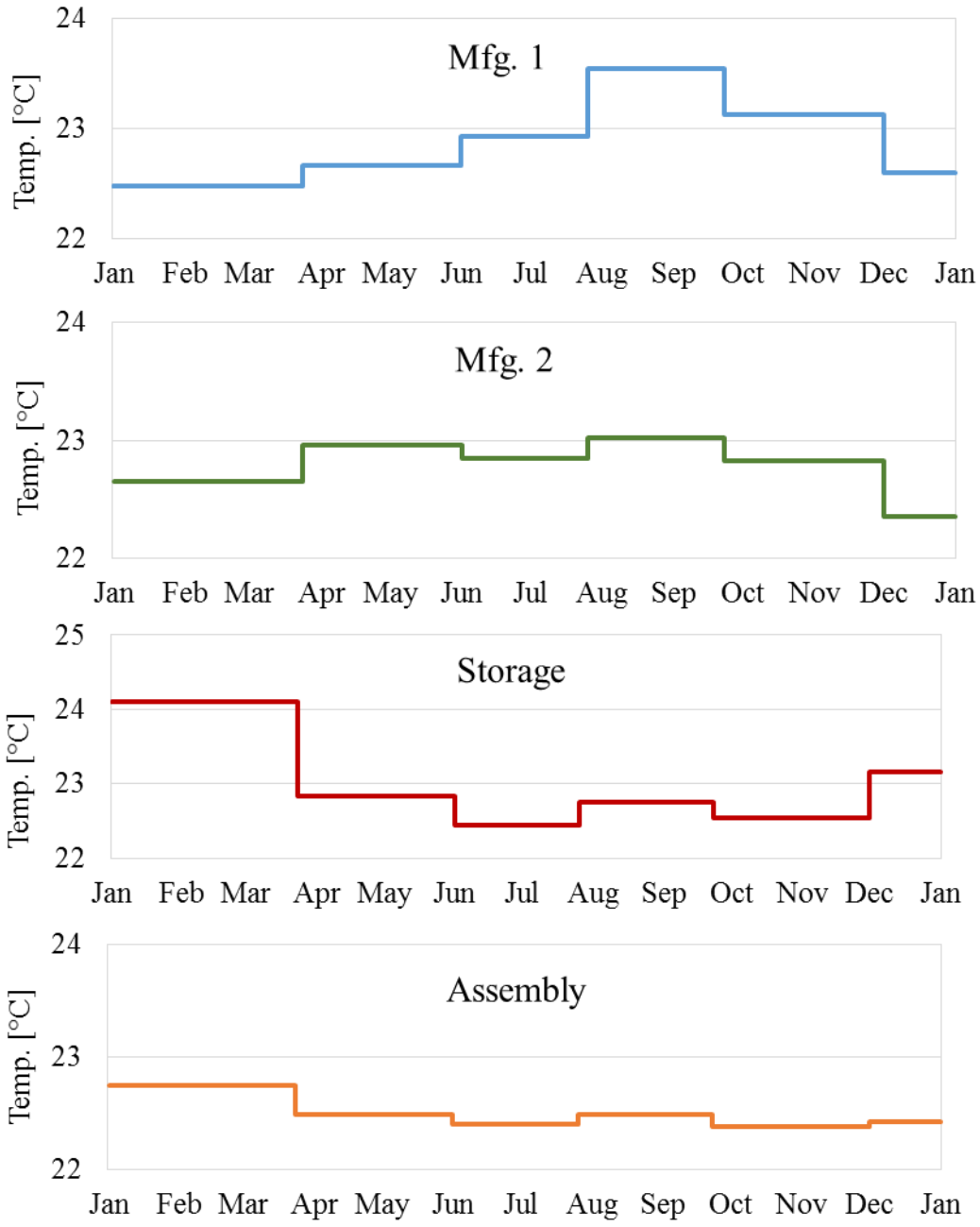

Figure 22: Input thermostat temperatures

Figure 22 shows the thermostat input temperature for each zone. Since the experiment collected vertical temperature profiles for a full year, a choice had to be made regarding discretizing the temperature profile inputs into EnergyPlus.

Theoretically, the measured temperature profiles could be averaged hourly and used as an hourly input to EnergyPlus. The difficulty with this approach lies in creating the schedule to control all 34,040 profiles (8,760 per room times 4 rooms). Another difficulty is removing 'misfit' data points. Since this approach requires much automation, a simple manual approach was taken.

The temperature profiles were discretized into six time slots and averaged over these time slots. The six slots can be seen in Figure 22. They are as follows:

Table 5: Temperature profile discretization time slots

Name	Start Date	Stop Date
Baseline Winter	January 1	March 23
Baseline Spring	March 24	May 31
Baseline Summer	June 1	July 25
XChanger Summer	July 26	September 22
XChanger Fall	September 23	November 30
XChanger Winter	December 1	December 31

These time slots were chosen to coincide roughly with the change from heating to shoulder season to cooling. XChanger was installed over two weeks in July, but it was assumed that the temperature profiles switch between baseline and XChanger on July 26, when the retrofit was completely finished.

4.3 Weather Data

For a building energy simulation that involves experimental validation, actual weather data should be used. The test site is conveniently located next to Baltimore-Washington International airport, which has a national weather service weather station onsite. The weather data is uploaded to the Integrated Surface Hourly Database. Notably, this database lacks solar radiation data required by EnergyPlus,

like diffuse horizontal and direct normal radiation flux. Since the online database is difficult to access, the data is difficult to format, the data has 'gaps' that require interpolation, and the data lacks solar radiation, numerous companies exist to access and format this data for the building energy simulation community. For this thesis, the data was purchased from one such company. The ASHRAE Clear Sky Model is one of several models that estimate the solar fluxes, whose values were included in the purchased weather file.

4.4 Schedules

The test facility operates as a typical manufacturing facility would be expected to operate. The building is occupied by roughly 40 people from 6:00 am – 5:00 pm. A standard work schedule has been assumed, with time given for lunch. Saturday has a single shift from 5:00 am – 1:00 pm. The facility is closed on Sundays.

Lighting is controlled manually by the occupants, with the exception of the occupancy controlled lighting in the offices. The shop lights are assumed to turn on at 6:00 am and off at 4:30 pm.

Electrical equipment, including manufacturing machines, the air compressor, and plug loads, are assumed to operate on the same schedule as each other. Since the test facility manufactures products from raw material, automated CNC machines are run continuously. These machines, roughly 7 out of 13 machines, or 54%, only stop running when they are reloaded with raw material. Therefore, the largest electrical load in the space is at 54% full capacity even when the building is unoccupied. The assumed schedule for the electrical loads on the shop floor is shown below.

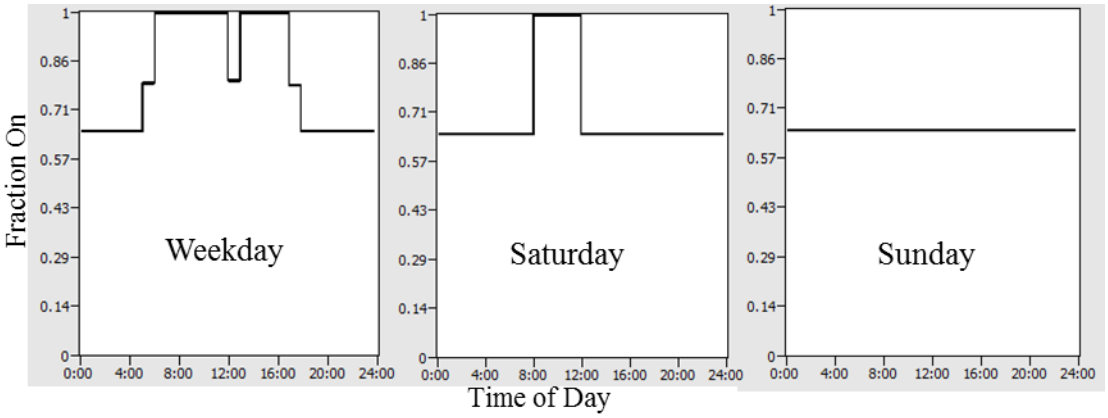

Figure 23: Manufacturing electrical equipment schedule

The building heating and cooling set points are usually set to 22.2 °C and are constant (i.e. no night time setback in heating season). Each rooftop unit has its own thermostat, implying that there are multiple (up to six) thermostats in each room. During site visits, thermostat set points were verified to be near 22.2 °C, but sometimes deviated by up to 1.2 °C. The thermostats are manually set to heating mode or cooling mode by the occupants to ensure that each room is entirely in heating or entirely in cooling. In other words, this ensures that a single room will not be both heated and cooled at the same time.

Infiltration is set to 'always on', which means that the EnergyPlus infiltration model operates continually. Additionally, a model for the opening and closing of garage doors has been developed. There is one garage door for the large manufacturing room and two doors in the storage room. Based on temperature data from nearby thermocouple poles, the doors open roughly twice a day around 8 am and 3:30 pm for five minutes. Therefore, the infiltration schedule for these rooms is set at 10% infiltration for when the doors are closed, and 100% infiltration when the doors are opened. In the infiltration modeling, infiltration rates have been determined

that create an appropriate infiltration flow rate for this schedule. See Section 4.8 for more information on infiltration.

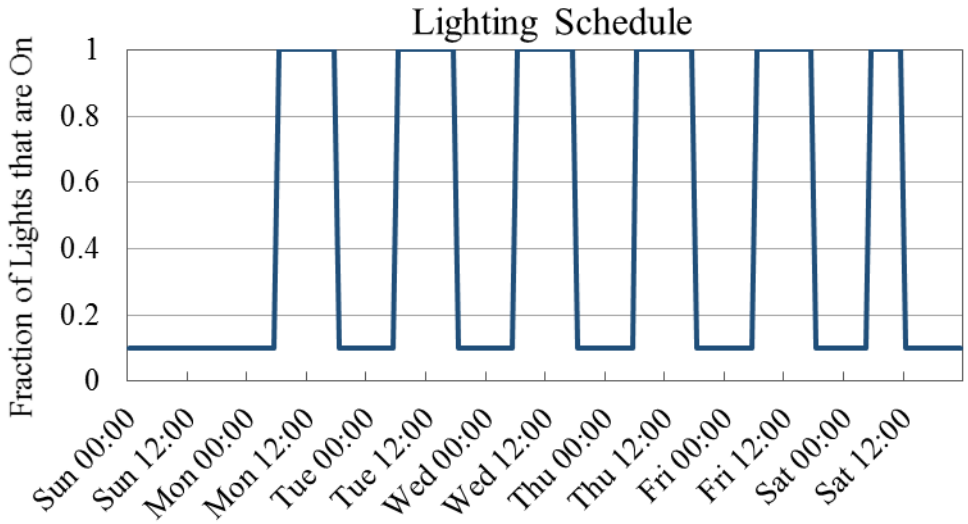

Figure 24: Lighting schedule

4.5 Electrical and Thermal Loads

4.5.1 Electrical Equipment

Estimating the power consumption and heat dissipation of the shop's electrical equipment is very important because the site's heating and cooling load depend on accurately accounting for the heat put off by the large CNC machines. The site is internally load-dominated, as shown in the Utility Bill Analysis. Some machines have dedicated heat exchangers and fans for cooling. Others have liquid coolant. Since there are so many different machines of different sizes and functionalities, the plug load for the manufacturing rooms was determined during calibration. It was determined that 35 W/m^2 is a reasonable plug load for these rooms. The air compressor in the large manufacturing room is treated as a separate plug load and

described in Section 4.9.3. As discussed in the model calibration section (see 5.3.1), plug loads were decreased to 17.5 W/m^2, a factor of 2, between May 4 and April 30.

The remaining plug loads were determined from an NREL report (Sheppy et al., 2014). The average office has a plug load of roughly 10 W/m^2. Since the office is actually two stories lumped into one zone, it is given a plug load of 20 W/m^2. The storage and assembly rooms have a plug load of 12 W/m^2. The equipment radiant fraction is 0.3 for all equipment.

4.5.2 Lights

The number of shop lights used in the factory is summarized in Table 6. The shop lights were replaced over a period from February 22, 2015 – March 15, 2015. The old lights, 400 W metal halide lights, were replaced by 190 W LED light fixtures. The metal halide light fixtures require 58 W for the ballast, so the entire fixture consumes 458 W. This value is consistent with the recommendations in ASHRAE Fundamentals (2005).

For a non-recessed light fixture, EnergyPlus calculates the convective heat from lighting fixtures as in (13).

$$Q_{conv} = 1 - Q_{radiative} - Q_{visible} \qquad \textbf{(13)}$$

The radiant light fraction is set at 0.42 and the visible light fraction is set to 0.18 based on the EnergyPlus documentation. Therefore, the convective heat fraction is 0.4. Although it is expected that LED lights have a higher visible light fraction than metal halide bulbs, the difference in heat transfer between visible and infrared is negligible from the heating calculation's perspective.

Table 6: Number of lighting fixtures in each room

Room	Large Mfg.	Small Mfg.	Storage	Assembly	Total
Number of Lights	33	25	21	66	145

4.5.3 Occupants

The production floor has roughly 20 workers at a time. According to ASHRAE Fundamentals (2005), an adult male give off 234 watts of heat doing light bench work in a factory setting. The 14 office worker give off 132 watts of heat each in moderately active office work. Therefore, the total heat load of the occupants is 6.5 kW at peak occupancy. The occupancy schedule is given in Section 4.4. Shift times were determined from a conversation with the site owner.

4.6 Building Envelope and Surface Constructions

4.6.1 Outer Walls

Since detailed site schematics were unobtainable, assumptions regarding the outer wall, inner wall, floor, and ceiling constructions are assumed based on material that is visible at the test site. The outer wall's construction is known to be a 0.46 m thick, four layer structure made of concrete blocks, rigid insulation, an air gap, and a brick façade.

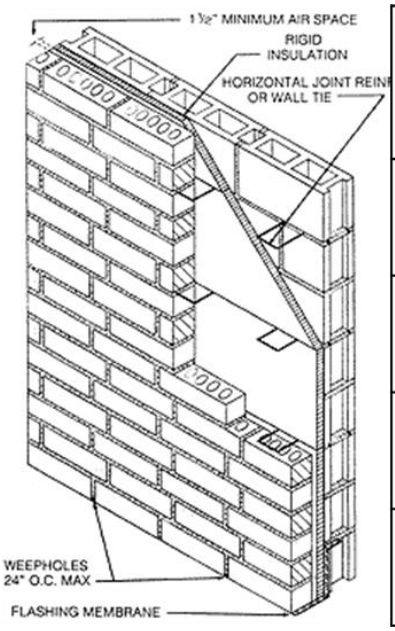

Material	Thickness [m]	Conductivity [W/m-K]	Density [kg/m^3]	Specific Heat [J/kg-K]
Concrete Block	0.203	0.98	1681	603
Rigid Insulation	0.1142	0.045	265	836
Air Gap	0.04	Thermal Resistance = 0.15 m2-K/W		
Brick	0.1016	1.02	2000	790

Figure 25: Wall insulation properties (source: Masonry Advisory Council)

4.6.2 Interior Walls and Open Doorways

The interior walls consist of either double-sided concrete block constructions or standard gypsum board constructions. Since these constructions are simple and relatively unimportant to the facility's energy use, they are not shown in detail here.

The offices take up two floors of roughly 12 offices, with a central hallway on each floor. This is not modeled fully due to its complexity. Instead, the office is modeled as a single story, open room with one central wall running down the middle. Since the offices are highly glazed, this wall ensures that the radiation from the windows transfers heat to the office, rather than to the walls in the adjacent rooms.

There exist large open doorways between the rooms of the shop floor. Some rooms have a motion-controlled vinyl doorway dividing them. This vinyl doorway is modeled in EnergyPlus as if it were a thin wall. The doorways that do not have the vinyl sheet are large, 'garage door' sized holes between the rooms. These doors are

modeled using the 'air wall' technique in EnergyPlus. An air wall allows for radiative heat transfer, but not conduction or convection between zones. Additionally, an air wall has no thermal mass. The test facility does have some airflow between rooms, so the fact that the air wall does not take into account convective heat transfer between zones is a source of error.

4.6.3 Floor

The site's floor is known to be a 0.25 m thick concrete slab. The concrete is a fiberglass reinforced type, called glass fiber reinforced concrete (GFRC). Hawileh examined the thermal properties of GFRC (2011). These properties are listed below. The EnergyPlus slab pre-processor was used to obtain ground temperatures.

Table 7: Thermal properties of concrete floor

Material	Thickness [m]	Thermal Conductivity [W/m-K]	Density [kg/m^3]	Specific Heat [J/kg-K]
Floor Slab (GFRC)	0.254	4.0	1600	1310

4.6.4 Roof Construction

The roof is assumed to be of the 'built-up' type. Its construction is shown in the image below, consisting of the corrugated metal roof deck, insulation, 'built-up' piles, and gravel. The thermal properties are given in Table 8.

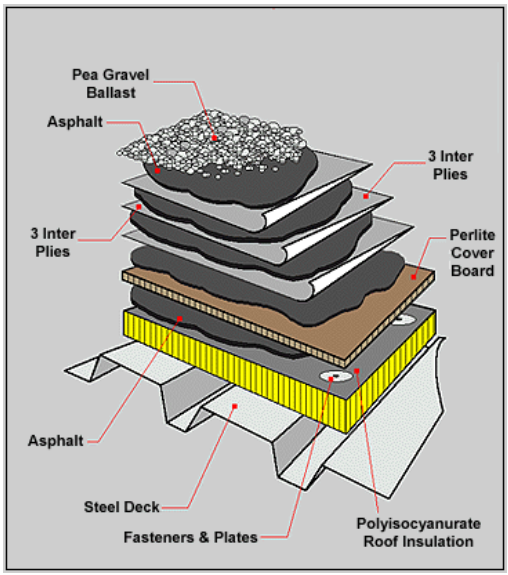

Figure 26: Built-up roof construction (source: Lydick-Hooks Roofing)

Table 8: Roof construction thermal properties

Material	Thickness [m]	Thermal Conductivity [W/m-K]	Density [kg/m^3]	Specific Heat [J/kg-K]
Roof Gravel	0.0127	0.38	881	1,674
Inter-piles	0.0095	0.162	1,121	1,464
Membrane	0.0095	0.2	800	1,000
Insulation	0.15	0.039	265	8,368
Decking	0.0015	45	7,680	418.4

4.7 Primary Systems (RTUs and air delivery)

The test facility is conditioned by rooftop units. These units have direct expansion cooling systems and gas heating systems. For a list of installed RTUs, see section 4.9 Retrofit Modeling. The offices are conditioned by two, 30 ton RTUs that send air to a variable-air-volume (VAV) system. Each particular office has a VAV box that determines the required air flow rate and reheat temperature (from electric heaters). Although each room in the test facility is served by multiple RTUs, there is no simple method in EnergyPlus to implement this. Therefore, each room is

conditioned by a single air loop that has the same capacity and flow rate as the actual room. Each air loop consists of seven components in the following order:

1. Space
2. Zone mixer – connects space to RTU
3. Outdoor air mixer – also called economizer
4. Cooling coil – direct expansion cooling
5. Heating coil – gas heating
6. Fan – single speed fan. VAV system has variable speeds
7. Zone splitter – connects RTU to space

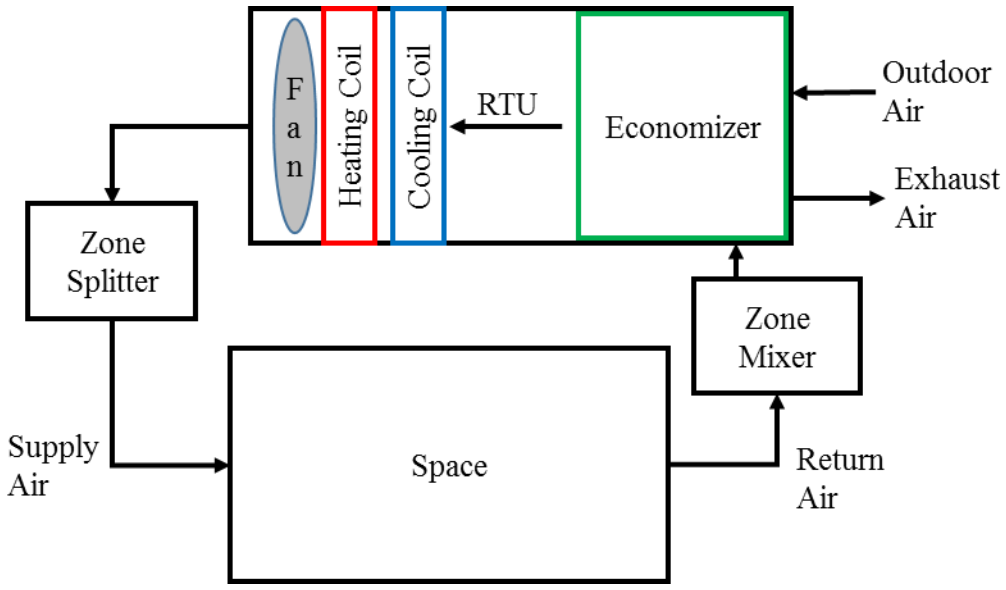

Figure 27: Typical air loop for a single space

4.7.1 Cooling Coil

The EnergyPlus object *Coil:Cooling:DX:SingleSpeed* was used to model the cooling coils before the retrofit. This object is provided with the room's total installed nominal capacity, rated air flow rate, average coefficient of performance (COP), rated sensible heat ratio, and a variety of performance curves. The performance curves are total cooling capacity as a function of return air wet-bulb temperature and outdoor dry-bulb temperature, cooling capacity as a function of flow fraction (actual air flow rate divided by rated air flow rate), the energy input ratio (inverse of COP) as a

function return air wet-bulb temperature and outdoor dry-bulb temperature, and the energy input ratio as a function of flow fraction.

These performance curves are biquadratic or quadratic curves. Since manufacturer's data only allows for the creation of the first two curves, the other two use default values in *OpenStudio*. The first curve was determined by applying least-squares regression on (14).

$$\dot{Q}_{cooling} = a + bT_{wb} + cT_{wb}^2 + dT_{amb} + eT_{amb}^2 + fT_{wb}T_{amb} \qquad \textbf{(14)}$$

The regression results produced the following coefficients.

a = 1.15
b = -0.00796
c = 0.00104
d = -0.00403
e = -3.2E-05
f = -0.00031

The resulting coefficients predicted nearly the same capacity as the default values in *OpenStudio* over a reasonable temperature range. This gives confidence to the use of the default coefficients in the other performance curves. Capacity as a function of flow fraction is given by (15).

$$\dot{Q}_{cooling} = a + b(ff) + c(ff)^2 \qquad \textbf{(15)}$$

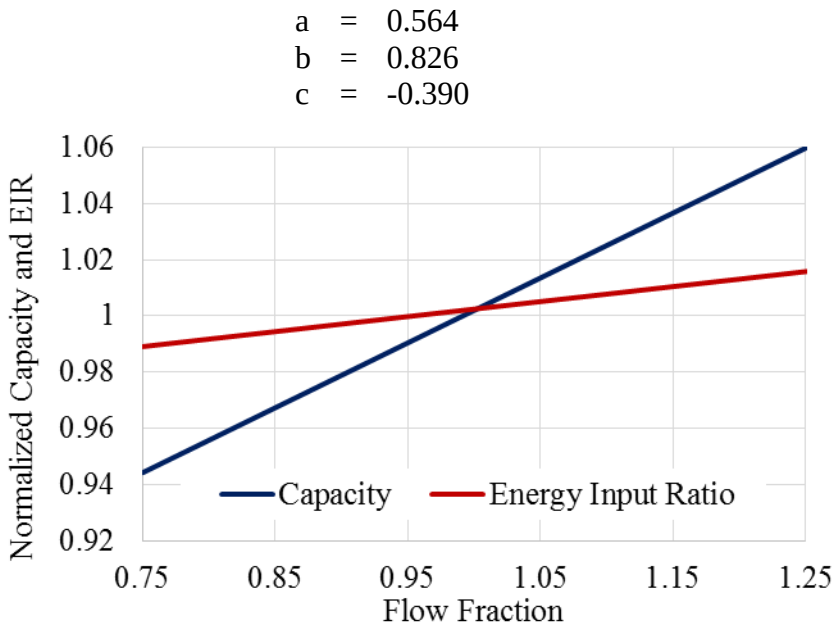

Figure 28: Quadratic performance curves for the RTUs

The facility had an RTU retrofit during the testing period. New, two-speed, high efficiency RTUs replaced the old, single speed units. The low speed compressor provides up to 55% full capacity. The air flow rate at low speed operation is assumed to also be 55% the full air flow rate. The same performance curves are used for low speed operation because reported performance data only contains two data points (at least three points are required for the least squares fit).

Control of two speed units is accomplished in a straightforward manner. If the cooling load is above zero but below the high speed capacity, then the unit operates in low speed mode. When low speed isn't providing enough capacity, then the unit operates in high speed mode. When low speed satisfied the load, then it cycles on and off like the single speed unit. This type of control is clearly a simplification of the actual unit's control because it requires that the unit knows the exact cooling load of the space, rather than thermostat information.

4.7.2 Heating Coil

The heating capacity for each coil was originally set to the actual total heating capacity installed in the room. A parasitic electricity consumption of zero is assumed. The furnace efficiency of both old and new RTUs is 0.81 from the manufacturer's literature.

In the actual test facility, each room is served by two to six RTUs. By default, gas heating coils in EnergyPlus operate at zero or 100 percent full capacity to meet heating demand. This results in cyclic overheating in the model that is not present in the actual space. Ideally, the EnergyPlus heating coils would have a part-load option (to deal with multiple RTUs being modeled by a single, large RTU). However, this is not easily implemented based on currently available objects. In other words, the heating performance in the model has no part-load performance, whereas each room in the test facility has part-load heating based on the number of RTUs in a given room.

4.7.3 Economizer Control

The economizers take the return and outdoor air to produce exhaust and supply air. Required outdoor air is set by specifying the required flow rate or flow fraction. Control over economizer availability, required outdoor air flow rate, and control scheme is provided to the user.

Some economizers in the test facility use enthalpy control while others use differential enthalpy control. Enthalpy control involves measuring temperature and RH of the outdoor air to calculate the enthalpy. This enthalpy then determines the conditions to impose on the control variable, the amount of outdoor air to take in.

Enthalpy control takes moisture into consideration, which is an improvement over dry-bulb temperature economizers. This ensures that the building will not become too humid.

The exact enthalpy and temperature limits of the RTU's economizer is not known because the manufacturer does not publish such information. Therefore, a typical control strategy has been created based on ASHRAE Standard 90.1 (2007). Maryland is in climate zone 4a where a fixed enthalpy high limit shutoff of 65,128 J/kg is recommended. This means that the outdoor air ratio will be set to the minimum allowed value when the outdoor air's enthalpy is greater than 65,128 J/kg. Differential enthalpy control does not require any user inputs because of the simple control logic – if the outdoor enthalpy is less than return air enthalpy, increase the outdoor air flow fraction.

Both enthalpy control and differential enthalpy control were implemented with a known value of 'minimum outdoor air ratio' of 10%. This means that, when free cooling is not possible, the building recycles 90% of its air with 10% coming from outside for ventilation. When free cooling is possible (according to economizer control), the controller increases the fraction of outdoor air (usually directly to 100%).

Although it is believed that the economizers were installed correctly at the test facility, the implementation of economizers in EnergyPlus results in different trends than the measured data shows. One possible reason for this is the fact that the manufacturing rooms are in cooling during much of winter (a fact that was verified at the test facility). Even with temperatures less than 0 ºC, the internal heat gains are so large that the manufacturing rooms require cooling. Therefore, the economizer in

EnergyPlus draws in outdoor air for cooling and the building consumes far less energy than the actual test facility uses in winter. The EnergyPlus model produces the same trends as the measured electricity consumption when economizer control is disabled during winter for the manufacturing rooms. Therefore, the economizer has been disabled for in the two manufacturing rooms (however, outdoor air ratio is constant at ten percent). The only economizer that is implemented is in the office, with an outdoor air fraction varying between 0.1 – 1.0 based on enthalpy control.

4.7.4 Fans

The XChanger ducting will require that the RTU indoor fan operates with a higher static pressure rise. Pressure drop can be broken between static, or friction pressure, and dynamic pressure. Using the friction pressure-loss diagram in McQuiston et al. (2004), a 0.45 m^2 duct providing 2.36 m^3/s (5000 CFM) produces a 4.5 Pa pressure drop per meter of duct.

Table 9: Fan Static Pressure Drop (McQuiston et al., 2004)

Evaporator Fan Static Pressure Drop (Pa)	
Filter	7.46
Economizer (10% outdoor air)	6.71
Baseline Ducting (2 m)	9
XChanger Ducting (8 m)	36
Loss Coefficients, K (dimensionless)	
90° Elbow	1.2
90° Elbow (vaned)	0.33
Supply Grille	0.36

$$P_v = \frac{1}{2}\rho v^2 = 77.76\ Pa \qquad \textbf{(16)}$$

$$P_{loss} = P_{static} + \sum K * P_v \qquad \textbf{(17)}$$

The baseline ducting contains one un-vaned bend, while the XChanger contains an average of three vaned bends and one un-vaned bends. Based on the manufacturer's specification for the average 12.5 ton RTUs used at the test facility, each fan with an XChanger unit will use nominally 1.47 kW while the baseline fans will use 0.78 kW.

Table 10: Total Pressure Loss in Ducts

Total Pressure Loss in Ducts (Pa)		
System	Baseline	XChanger
Static	23.2	50.2
Dynamic	121.3	198.2
Total	**144.5**	**248.4**

Table 11: EnergyPlus Fan Object Inputs

EnergyPlus Two-Speed Fan Inputs	
Pressure Rise	144.5 (baseline), 248.4 (XChanger)
Fan Total Efficiency	0.7
Minimum Flow Fraction	0.3
Motor Efficiency	0.93
Power Part Load Fraction	PLF = .0013+.147ff+0.9506ff ^{2}-.0998ff ^{3}

EnergyPlus needs a power part load fraction as a function of flow fraction curve. When sufficient data from the manufacturer is not available to generate a performance curve, the curve should be taken from ASHRAE Standard 90.1 – 2013 appendix G. This is plotted below.

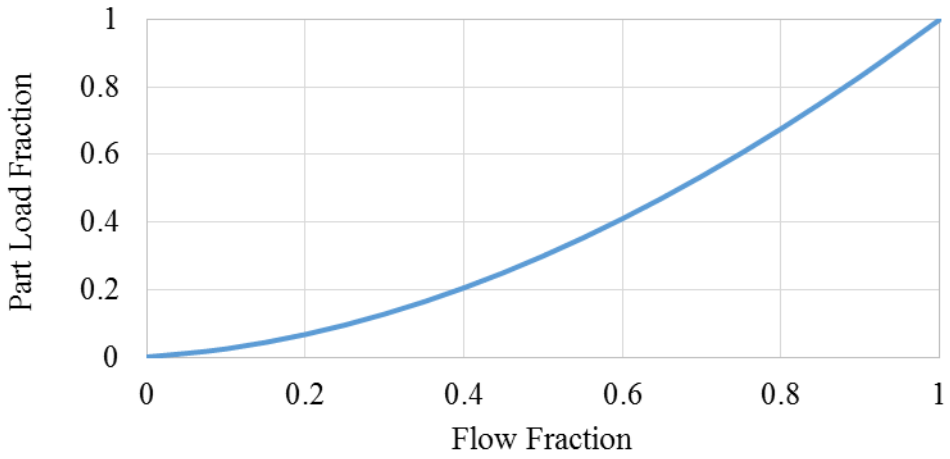

Figure 29: Fan part load power as a function of flow fraction

4.8 Infiltration

In EnergyPlus, infiltration is modeled as a function of wind speed and temperature difference given by (18).

Clearly, this equation lacks vertical wind speed variation, wind direction, and envelope properties like crack sizes and porosity. These properties are assumed to be lumped into I_{design}. In a DOE report, Gowri et al. (2009) recommended the use of the default BLAST coefficients given below with an I_{design} value of 0.001024 m^3/s per exterior wall area.

$$\dot{V}_{infiltration} = I_{design} F_{schedule} \left(A + B\left|T_{zone} - T_{db,amb}\right| + CV_{wind} + DV_{wind}^2\right) \quad \textbf{(18)}$$

where

A = 0.606
B = 0.0364
C = 0.118
D = 0

The large manufacturing room and the storage room each have large bay doors that open roughly twice per day. The response of the indoor vertical temperature profile can be observed from the nearest pole to the door, 6.1 m away.

Figure 30 shows the opening of a bay door in the large manufacturing room on February 15, 2016. The outdoor air temperature was 0.6°C and the wind speed was 10.8 m/s from the west (this building face is oriented towards the southwest).

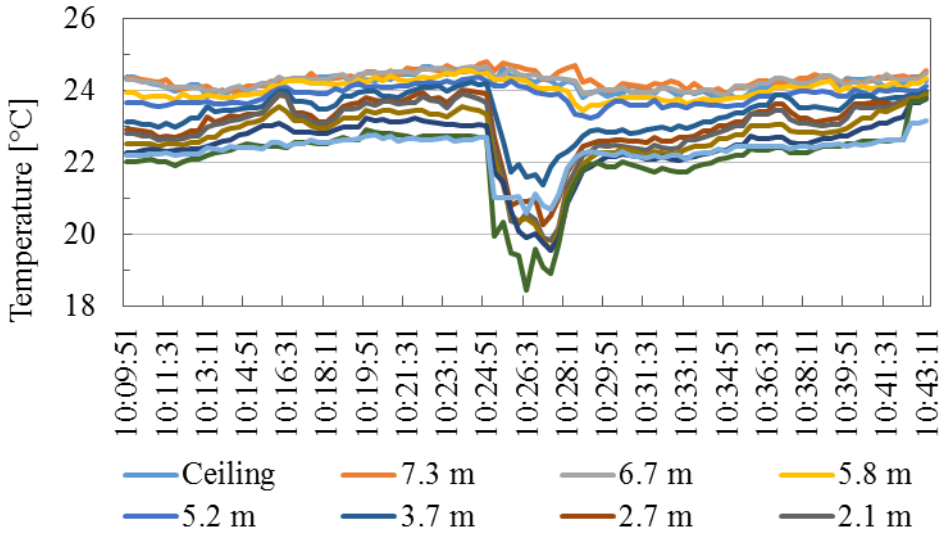

Figure 30: Temperature profile measured during bay door opening

The bay door opening is modeled in EnergyPlus using infiltration. The advantage of modeling the bay door opening using an infiltration object is that wind speed is considered when calculating flowrate. Though the doors open at different times each day, it is assumed in the model that they open at 8 am and 3:30 pm for five minutes Monday through Friday. The air change rate due to infiltration can be seen in Figure 31. Additionally, each room receives at least ten percent outdoor air through mechanical ventilation.

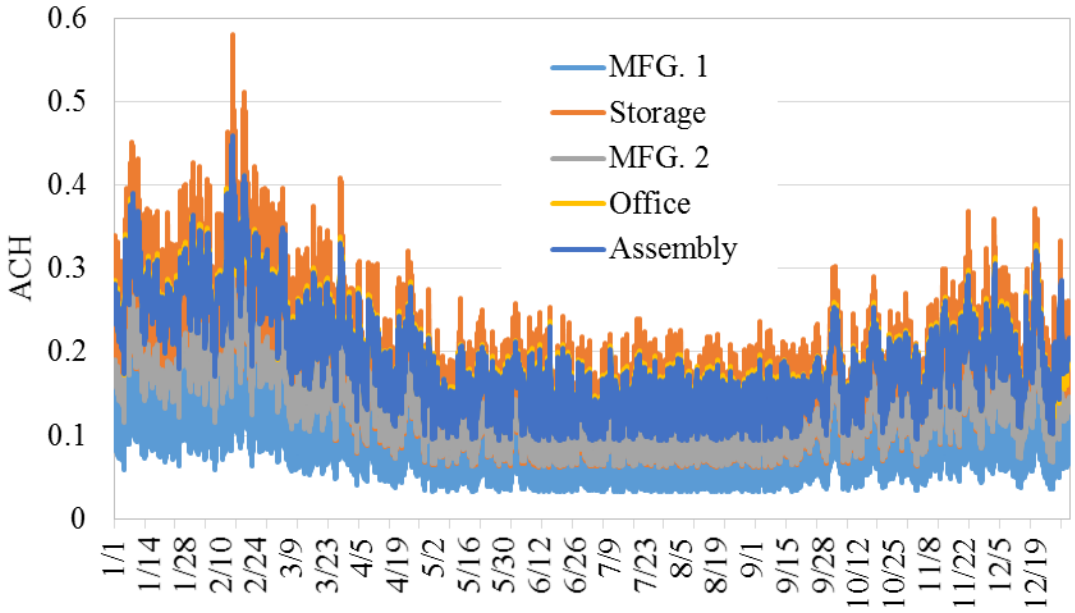

Figure 31: Air change rate due to infiltration

4.9 Retrofit Modeling

4.9.1 Lights

The test facility underwent a lighting retrofit on the shop floor, switching from metal halide bulbs to LED lights. The lighting electric and heat load are estimated according to Section 4.5 of this thesis. Building the retrofit into EnergyPlus is straightforward using scheduling to assign a given light object to be 'on' when appropriate.

The lighting was replaced over the course of roughly three weeks. In the simulation, each room switches from the old to new lights in a single day. Therefore, the smooth, linear decrease in power consumption that the facility saw over the three week installation period can be approximated by the model (as opposed to a simple one-day switchover).

4.9.2 Rooftop Units

The test facility's RTUs were retrofitted according to Table 12. The units serving the manufacturing rooms, the rooms with the highest cooling demand, had an average COP improvement from 2.56 to 3.58. The entire facility average COP improved from 2.92 to 3.44. An additional 151 kW of gas heating capacity and 35 kW of cooling capacity were added to the facility. Upgrading the RTUs also introduces two stages of cooling through the use of dual compressors. Both old and new units use air-side economizers with enthalpy control. Therefore, it is assumed that the economizer behavior is identical before and after the retrofit.

Table 12: Rooftop unit specifications before and after retrofit

Test Facility RTU Summary [NEW] [OLD] [UNCHANGED]												
Unit	Manufacturer	Cooling [Tons]	Heating [Btu/h]	EER	COP	Description	Area Served	Manufactured	Refrigerant	Model #	Serial #	Status
1	TRANE	30	486,000	11.0	3.22	DX, VAV	Office	Mar-2010	R-410A	YCD360B4HC2B6DD	C10001446	
2	TRANE	4	243,000	9.7	2.84	DX, CV	Mfg 2	Sep, 2005	R-22	YHC048A		
3	TRANE	12.5	250,000	12.1	3.55	DX, CV	Mfg 1	May, 2015	R-410A	YHD150G4RHA01H00	152010096D	
	York		161,500	8.75	2.56			May-1997	R-22	D4CG150N16546JSC	NEFM058047	
4	TRANE	12.5	250,000	12.1	3.55	DX, CV	Mfg 1	May, 2015	R-410A	YHD150G4RHA01H00	152010096D	
	York		161,500	8.75	2.56			May-1997	R-22	D4CG150N16546JSC	NEFM058043	
5	TRANE	10	161,500	12.4	3.63	DX, CV	Mfg 2	May, 2015	R-410A	YHC120E4RMA11H00	151311104L	
	York			8.75	2.56			May-1997	R-22	D3CG120N16546JSD	NEFM064821	
6	TRANE	12.5	250,000	12.1	3.55	DX, CV	Mfg 1	May, 2015	R-410A	YHD150G4RHA01H00	152010096D	
	York		161,500	8.75	2.56			May-1997	R-22	D4CG150N16546JSC	NEFM067221	
7	TRANE	15	300,000	12.1	3.55	DX, CV	Mfg 1	May, 2015	R-410A	YHD180G4RLA01H00	152101390	
	York			8.75	2.56			Jun-1997	R-22	D2CG180N24046ECE	NFFM067221	
8	TRANE	10	161,500	12.4	3.63	DX, CV	Mfg 2	May, 2015	R-410A	YHC120E4RMA11H00	151311104L	
	York			8.75	2.56			May-1997	R-22	D3CG120N165461SD	NEFM064803	
9	TRANE	12.5	250,000	12.1	3.55	DX, CV	Storage	May, 2015	R-410A	YHD150G4RHA01H00	152010096D	
	York		161,500	8.75	2.56			Apr-1997	R-22	D4CG150N16546JSC	NDFM045467	
10	TRANE	8.5	129,400	12.5	3.66	DX, CV	Machine	May, 2015	R-410A	TYSC102F4EMA001SC	-	
	York			8.75	2.56			May-1997	R-22	D3CG102N130461SF	NEFM064209	
11	TRANE	10	161,500	12.1	3.55	DX, CV	Machine	May, 2015	R-410A	YHD150G4RHA01H00	152010096D	
	York			8.75	2.56			Apr-1997	R-22	D4CG150N16546JSC	NDFM045467	
12	TRANE	30	283,500	11.0	3.22	DX, VAV	Office	Sep-2005	R-22	YCD330A4LR2A6DE4	CO5H07554	
3W	TRANE	6	64,000	11.5	3.37	DX, CV	Assembly	Sep-2005	R-22	YHC072A4RLA1R	5361026081	
4W	TRANE	6	64,000	11.5	3.37	DX, CV	Assembly	Sep-2005	R-22	YHC072A4RLA1R	5361028351	
5W	TRANE	6	64,000	11.5	3.37	DX, CV	Assembly	Sep-2005	R-22	YHC072A4RLA1R	5361029071	
6W	TRANE	6	64,000	11.5	3.37	DX, CV	Assembly	Sep-2005	R-22	YHC072A4RLA1R	536102761L	
7W	TRANE	6	64,000	11.5	3.37	DX, CV	Assembly	Sep-2005	R-22	YHC072A4RLA1R	536102610L	
8W	TRANE	6	64,000	11.5	3.37	DX, CV	Assembly	Sep-2005	R-22	YHC072A4RLA1R	536102981L	
13	TRANE	6	96,000	11.2	3.28	DX, CV	Storage	May, 2015	R-410A	TYSC072F4EMA001ST	-	
14	TRANE	4	65,600	13.0	3.81	DX, CV	Mfg 2	May, 2015	R-410A	TYSC048E4EMA001ST	-	

To implement the RTU retrofit in EnergyPlus required adding another coil in the air loop. Then, 'on/off' availability schedules are used to ensure the required coil

is on or off when it should be. The presence of an extra cooling coil in an air loop has no effect on the air stream when the coil's status is 'off'.

4.9.3 Air Compressor

The test facility uses an industrial air compressor to supply compressed air for manufacturing purposes. This compressor was replaced on October 14, 2015 with a unit that uses 10 hp less electricity (7.4 kW). The efficiency of the old compressor was not listed, so its heat output was calculated assuming the same efficiency as the new compressor.

The energy consumption of industrial compressors using load/unload-type control can be calculated in the manner provided by the Department of Energy (2013). In the 35 days since installation, the air compressor was fully-loaded for 263 hours, or 31.3% of the time. To make the energy consumption calculation possible, it is assumed that the unit operates either fully-loaded or fully-unloaded, the unloaded capacity is 25% fully-loaded capacity, and the old compressor run-time was the same as the new compressor. The result of this calculation is time averaged electricity consumption of 21.7 kW for the old compressor and 18.1 kW for the new compressor. From the manufacturer's specifications, 94.4% of the input electricity is dissipated as heat to the space.

The compressor is cooled using space air inside of its internal heat exchanger. To save heating costs during winter, this hot air is directed back into the space. During the other seasons, this air is exhausted outside. The date to switch from indoor exhaust to outdoor exhaust was chosen based on when the site switches between heating and cooling. This information is summarized in the following table. It should

be noted that the switch to heating was late, December 15, due to an unseasonably warm December in 2015.

Table 13: Air compressor model status

Date	Air Compressor Model	Power Consumption [kW]	Fraction of Heat Loss to Ambient
Jan 1 – Feb 15, before retrofit	Old compressor exhaust to space	21.7	0
Feb 16 – Oct 14, before retrofit	Old compressor exhaust to ambient	21.7	1
Oct 15 – Dec 15, after retrofit	New compressor exhaust to ambient	18.1	1
Dec 16 – Dec 31, after retrofit	New compressor exhaust to space	18.1	0

5. Results Analysis and Discussion

5.1 Experiment

5.1.1 Temperature Profiles

Temperature measurements were averaged for each thermocouple over each season before and after the XChanger retrofit and shown in Figure 33. The legend corresponds to the following map.

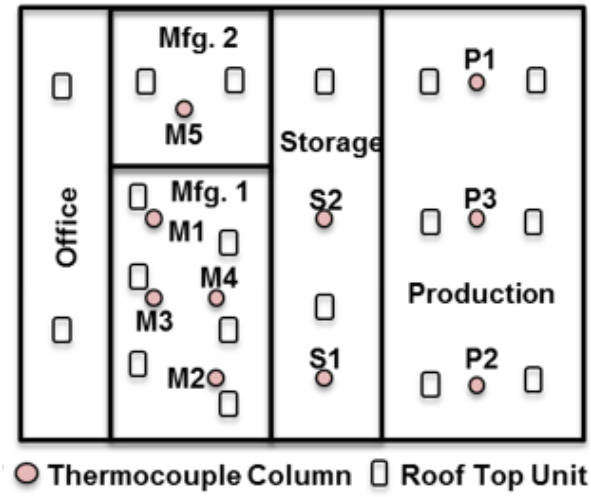

Figure 32: Map for thermocouple column naming

Figure 33 shows that temperatures vary insignificantly in the x-y direction within a single room. Any horizontal temperature gradient is due to the RTUs being controlled by their own thermostat, which means that some parts of a room receive more cooling than others. In the large manufacturing room, column M2 has significant stratification near the ceiling in each season. This is due to its location near several large CNC machines and the industrial air compressor.

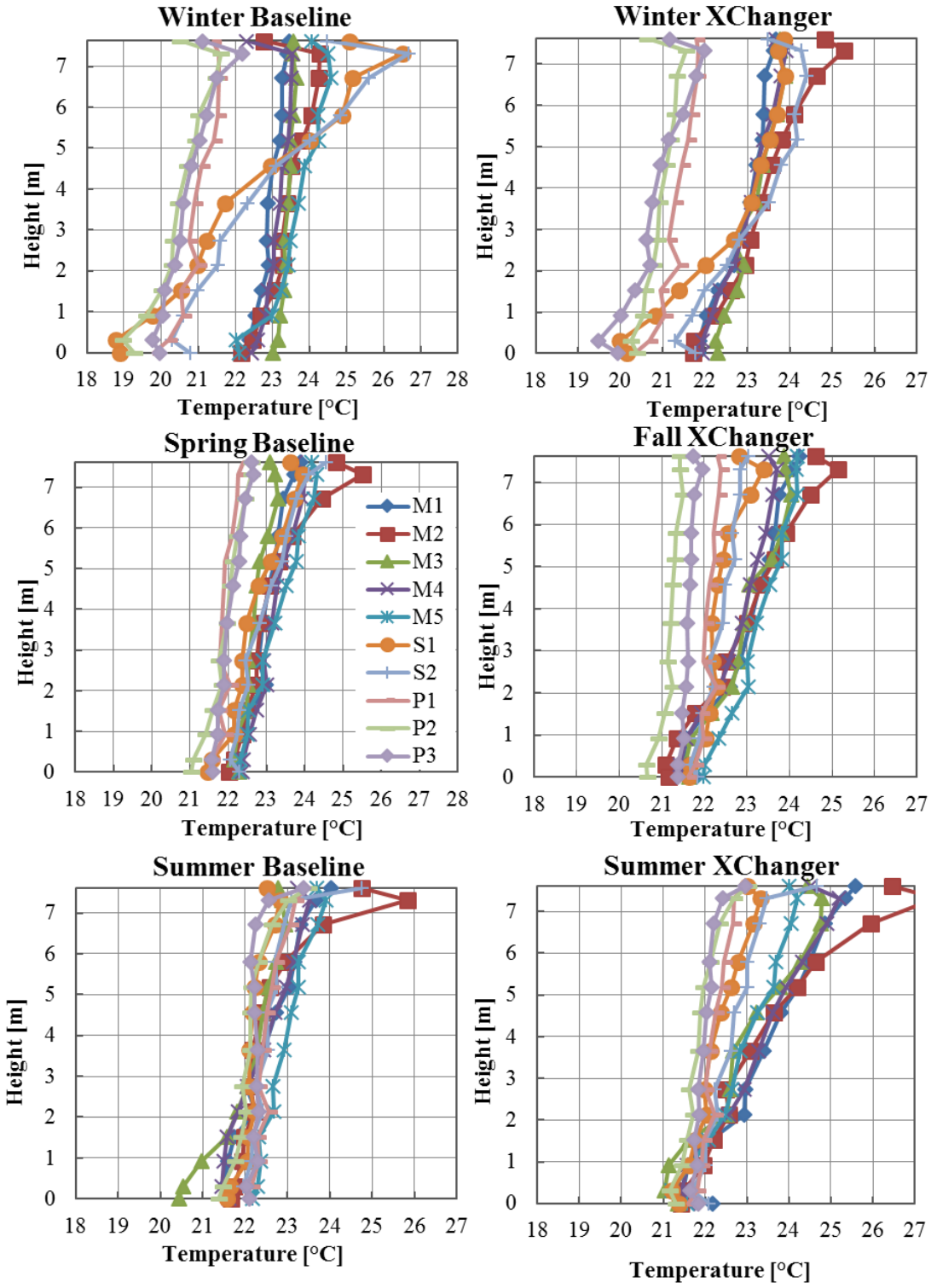

Figure 33: Average seasonal temperature of each thermocouple

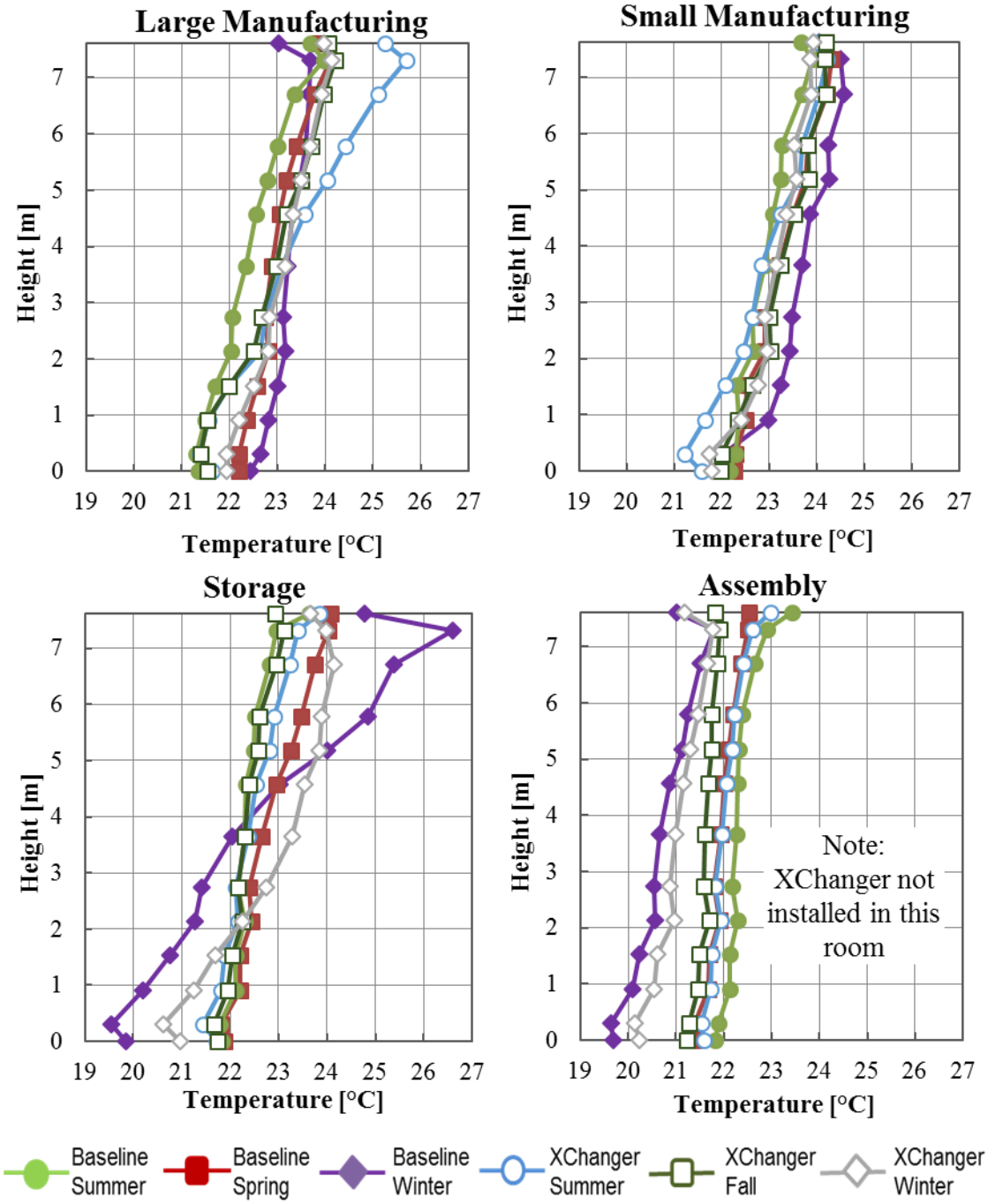

Figure 34: Average measured temperature profile by room

Since horizontal temperature gradients within each room were not significant, the thermocouple poles have been averaged by room for clarity in Figure 34. Since

the assembly room did not have any change in the ducting, there are very little changes before and after the retrofit.

During the summer, the manufacturing rooms have almost continuous cooling and therefore saw the greatest change under the XChanger retrofit. In the large manufacturing room, XChanger maintained the same temperature in the occupied zone while increasing the stratification in the upper zone by 1.8 K. In the small manufacturing room, the temperature in the occupied zone decreased while the temperature in the upper portion of the space increased. Since the storage room has a low cooling load, the RTUs are not on very often. Therefore, the storage room had no significant change in temperature profile during cooling season.

During the winter, however, the storage room realized the greatest benefit from XChanger. The baseline winter had the greatest observed stratification in the building – 7.1 K. Supplying air high and returning air above the occupied zone reduced the temperature stratification to 3.5 K, a reduction of 50%. In particular, the sharp gradient near the ceiling was reduced. The other rooms saw a negligible difference during heating season. One possible explanation for this is that the manufacturing rooms were in cooling for portions of the winter. One piece of evidence to justify this claim is that the XChanger winter profile resembles baseline summer (which both had high supply ducts) in their shape, especially near the ceiling.

During spring and fall, XChanger produced different effects in each room. In the large manufacturing room, the temperature below 2 m was reduced by 1 K, while the upper zone remained the same. In the storage room, the effect was the exact

opposite, with 1 K stratification near the ceiling and the same temperature in the occupied zone. The small manufacturing room had no change whatsoever.

5.1.2 Utility Bill Analysis

Utility bills were obtained from January 2014 through March 2016. Since 2014 had no retrofits, it will act as a baseline to examine the four retrofits installed in 2015: LED lights in February, higher efficiency RTUs in June, XChanger in July, and the air compressor in October.

Table 14: Monthly electricity and gas consumption before and after retrofits

Electricity Consumption [MWh]				
Month	2014	2015	Difference	Reduction
Jan	177.7	173.6	4.0	2.3%
Feb	159.7	165.3	-5.7	-3.6%
Mar	152.3	130.8	21.5	14.1%
Apr	166.9	137.4	29.5	17.7%
May	158.3	125.9	32.4	20.5%
Jun	165.2	145.9	19.3	11.7%
Jul	176.2	122.3	53.9	30.6%
Aug	166.1	125.7	40.5	24.3%
Sep	168.6	137.5	31.1	18.5%
Oct	157.6	117.7	39.9	25.3%
Nov	123.3	113.0	10.2	8.3%
Dec	148.1	112.4	35.6	24.1%
Total	1919.8	1607.5	312.3	16.3%
Gas Consumption [Therms]				
Month	2014	2015	Difference	Reduction
Jan	2,065	1,979	86	4.2%
Feb	2,176	1,916	260	11.9%
Mar	1,666	1,729	-63	-3.8%
Apr	1,133	1,000	133	11.7%
May	663	180	483	72.9%
Jun	156	46	110	70.5%
Jul	18	8	10	55.6%
Aug	24	8	16	66.7%
Sep	31	22	9	29.0%
Oct	99	133	-34	-34.3%
Nov	730	490	240	32.9%
Dec	1,325	1,002	323	24.4%
Total	10,086	8,513	1,573	15.6%

Based on Table 14, the facility had an average electricity savings of 16.3% and average gas savings of 15.6% in 2015. The electricity savings peaked at 30.6% during the hottest month, July. Since no retrofits were installed during January through the third week in February, those months saw only a small change in energy use that can be attributed to changes in plug load and other random variables. These

values do not account for weather differences between 2014 and 2015. It was attempted to normalize gas and electricity use by degree days.

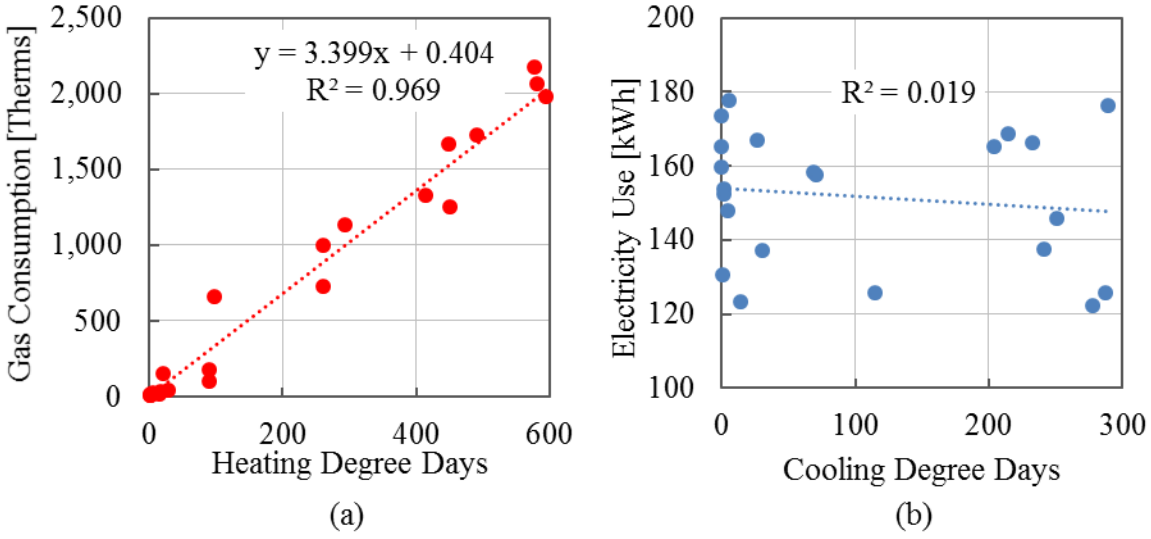

Figure 35: Monthly degree day regression for (a) heating, (b) cooling

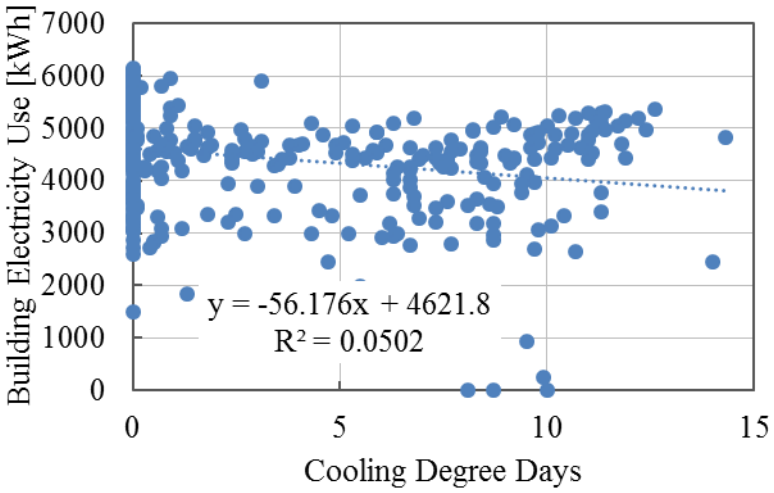

Figure 36: Degree day normalization for daily data

Since the facility only uses natural gas for space heating, the gas use correlates very well with heating degree days, with an R^2 of 0.97. The electricity use, however, does not correlate with cooling degree days on a monthly or daily basis, implying that the building is dominated by internal loads, rather than external loads.

Although electricity does not correlate with ambient dry-bulb temperature, the energy savings of Table 14 gain credibility by considering that 2015 was warmer in every month of the year than in 2014. Based on ambient temperature, the results can be considered conservative. However, other uncertainties such as building use and plug load cannot be accounted for either.

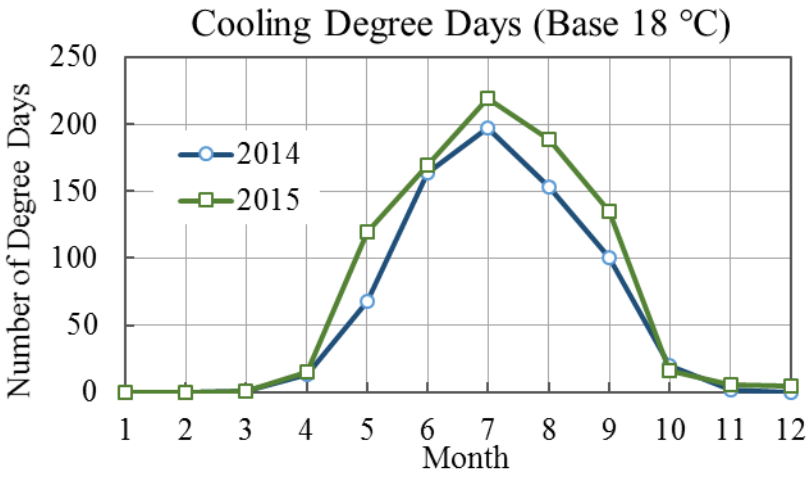

Figure 37: CDD increase from 2014 (baseline) to 2015 (post-retrofit)

The energy savings of the lighting can be calculated directly. The results are given in Table 15. The results agree with the values simulated using EnergyPlus, in Table 17.

$$E_{light} = Ptf \quad \textbf{(19)}$$

$$E_{facility} = E_{light} + \frac{E_{light}}{COP} \quad \textbf{(20)}$$

where

E_{light} = light's electricity use [kWh]
P = light's rated power consumption [kW]
t = time period of interest [h]
f = Use Factor, average value of light schedule
$E_{facility}$ = facility's extra electricity use due to the light [kWh]
COP = coefficient of performance for vapor compression cycle [-]

Table 15: Yearly energy savings of switching from metal halide to LED bulbs

Light Fixture	Power [W]	Use Factor	Number of Lights	Energy per Bulb [kWh/bulb/year]	Energy per 30 Days [kWh]	Energy per Year [kWh]
Old	458	0.41	145	1,771	21,104	256,767
New	190			735	8,755	106,519

The energy savings of the higher SEER RTUs has been simulated in EnergyPlus using the validated 2015 model. The energy savings are shown in the following table.

Table 16: RTU retrofit energy savings

Energy Savings due to Rooftop-Unit Retrofit [MWh]												
Period Beginning In:	Jan	Feb	Mar	Apr	May	Jun	Jul	Aug	Sep	Oct	Nov	Total
Old RTUs	146	129	128	117	141	133	130	139	116	108	111	1771
New RTUs	146	128	126	114	135	126	126	135	115	107	110	1740
Energy Saved Per Month												2.56
Energy Saved per Summer Months												4.88

Using the monthly calculated savings due to the lighting and RTU retrofits, the energy savings due to XChanger can be estimated according to (21).

$$XChanger\ Energy\ Savings = E_{2014} - E_{2015} - \Delta E_{Lights} - \Delta E_{RTU} - \Delta E_{Compressor} \quad \textbf{(21)}$$

The lighting, RTU, and air compressor retrofit energy savings were calculated through simulation using the validated 2015 EnergyPlus model. Each retrofit was modeled as if it were the only retrofit installed in the facility. Then, the results were compared with a baseline model that does not have that specific retrofit. Fluctuations in the value of the difference in energy consumption between the two years can only be explained by considering outdoor temperature, manufacturing output, and other variables that are not controlled for.

Table 17: Electricity savings due to XChanger calculated from utility bills

					Electricity Savings due to:			
Start	Stop	2014 [MWh]	2015 [MWh]	Energy Savings	Lights	RTU	Compressor	XChanger
1/23	2/20	160	165	-3.6%	-	-	-	-
2/20	3/20	152	131	14.1%	9.6%	-	-	-
3/20	4/22	167	137	17.7%	11.0%	-	-	-
4/22	5/20	158	126	20.5%	11.7%	-	-	-
5/21	6/20	165	146	11.7%	11.4%	-	-	-
6/20	7/22	176	122	30.6%	10.6%	5.1%	-	14.9%
7/22	8/21	166	126	24.3%	11.9%	3.2%	-	9.3%
8/21	9/21	169	137	18.5%	11.1%	2.7%	-	4.7%
9/22	10/21	158	118	25.3%	11.8%	1.4%	-	12.1%
10/21	11/19	123	113	8.3%	12.1%	0.7%	2.3%	-6.9%
11/19	12/18	148	112	24.1%	11.5%	0.8%	2.3%	9.5%
12/18	1/21	174	132	24.1%	11.0%	0.3%	2.0%	10.8%
Start	Stop	2015 [MWh]	2016 [MWh]	Energy Savings	Lights	RTU	Compressor	XChanger
1/21	2/19	165	126	24.0%	10.5%	0.6%	2.0%	10.9%
2/19	3/22	131	129	1.0%	10.2%	0.6%	1.9%	-11.6%

The gas use for space heating correlates very well with heating degree days. Therefore, it makes sense to compare gas usage per heating degree day. However, to compare the gas used in 2015 against 2014, the heat load of the lighting and compressor retrofits must be added back because the lower electrical loads seen in 2015 mean that the facility needs more gas for space heating. Using the validated 2015 EnergyPlus model, it was found how much heat would have been added to the space had each retrofit not occurred. This heat was converted to a "therm equivalent" by converting Joules (EnergyPlus output) to therms, then dividing by the efficiency of the gas furnace, 0.81. Since the heat output difference due to the compressor retrofit

is less than six therms equivalent for each period, it was ignored for simplicity. Summer months were included for completion, but the results are omitted because a negative therms-per-degree-day was calculated.

One source of error in this analysis is that 'adding back' the heat due to the lighting retrofit is correct only when the facility is in heating operation during the entire period considered. This is the reason that the shoulder seasons and summer had negative therms-per-degree-day in 2015. This is also the reason that the calculated 'Difference' increases from 1/23/14 – 3/20/14. A better approach would include the fraction of time the facility spent in heating. However, this is not readily available from the experiment or as an EnergyPlus output variable.

The XChanger was switched from cooling operation (supply low, return high), to heating operation (supply high, return low) on January 4, 2016. Therefore, half the period from 12/18/15 – 1/21/16 and the whole period from 1/21/16 – 2/19/16 are direct comparisons between baseline and XChanger systems. During these periods, the XChanger saved 0.7 therms per heating degree day. This is a savings of 20.1 – 22.3% gas. However, this analysis is clearly subject to large uncertainties, as shown in the first row when no retrofits were installed, yet the facility observed a difference in therms-per-degree-day of 0.58.

Table 18: Facility gas consumption before and after retrofits

Start	Stop	2014 [Therms]	2015 [Therms]	2015 Adjusted for Lights	HDD 2014	HDD 2015	2014 Therms / HDD	2015 Therms / HDD	Difference
1/23	2/20	2,176	1,916	-	576.6	600.3	3.77	3.19	0.58
2/20	3/20	1,666	1,729	1149	448.5	490.7	3.71	2.34	1.4
3/20	4/22	1,133	1,000	331	293.4	266.9	3.86	1.24	2.6
4/22	5/20	663	180	-474	98.1	86.8	6.76	-	-
5/21	6/20	156	46	-703	20.1	26.8	7.76	-	-
6/20	7/22	18	8	-616	2.5	1.1	7.20	-	-
7/22	8/21	24	8	-702	6	1.7	4.00	-	-
8/21	9/21	31	22	-679	17.7	14.5	1.75	-	-
9/22	10/21	99	133	-507	89.6	119.5	1.10	-	-
10/21	11/19	730	490	-128	261.5	166.5	2.79	-	-
11/19	12/18	1,325	1,002	396	415.2	294.4	3.19	1.34	1.9
12/18	1/21	1,979	1,819	1268	594.8	475.7	3.33	2.66	0.7
Start	Stop	2015 [Therms]	2016 [Therms]	2016 Adjusted for Lights	HDD 2015	HDD 2016	2015 [Therm / HDD]	2016 [Therm / HDD]	Difference
1/21	2/19	1,916	1,878	1327	600.3	535.4	3.19	2.48	0.7
2/19	3/22	1,729	1,094	579.8	514	490.7	315.6	3.52	1.63

Since the characteristics of this particular facility may differ from other commercial buildings, it is beneficial to view the energy savings as a percentage of total HVAC energy use. A watt-meter was placed on one electric panel to measure the power consumption of a collection of rooftop-units serving both manufacturing rooms and the storage room. The office and assembly spaces were not instrumented. 52.4% of installed cooling capacity was instrumented starting on July 31. Between July 31 and September 24 (roughly the end of cooling season), the instrumented RTUs consumed 41,089 kWh. Assuming that the cooling load is distributed evenly throughout the facility, the entire facility will use 78,415 kWh over the same period. Based on Table 17, the XChanger system saved the facility 7.0% energy in August

and September. Since the entire facility consumed 237,592 kWh during this period, the XChanger system saved the facility 16,631 kWh.

Had the storage and manufacturing rooms not been installed with XChanger, they would have used 41,089 + 16,631 kWh, or 57,720 kWh. Compared to what they actually used, 41,089 kWh, XChanger saved these rooms 28.8% of HVAC energy. Implicit in this figure is the assumption that the cooling load is distributed evenly throughout the space. This assumption is necessary to estimate the energy consumption of the facilities RTUs.

Based on this analysis of the utility bills, the XChanger system is expected to save 9.6% total electricity, which is 28.8% of HVAC energy during cooling season. During heating season, XChanger is expected to save 21.2% gas during heating season.

5.2 CFD Modeling

5.2.1 Grid Sensitivity Analysis

Based on the initial simulations and literature review, a mesh of 750,000 cells was selected. This grid was capable of producing y* values within the boundaries defined by the wall-treatment, 30-300. Table 2 from the introduction shows the grid density used by other researchers with similar physics and models, particularly natural convection and k-ε turbulence modeling. Although grid density is not as important as y* values for heat transfer or as important as local grid considerations, like the grid near outlet diffuser, overall grid density is used here as a qualitative initial benchmark. The reviewed literature typically had between 1,000-12,000 cells/m^3. Denser grids typically corresponded to more ‘theoretical’ studies that focus

on a specific, local aspect of the simulation, like detailed heat transfer or detailed diffuser configurations. Denser grids were also used for studies that had detailed geometry and rigorous experimental data. Coarser grids typically correspond to situations with less well-known boundary conditions or where the simulation goal is of a larger scale, such as the mean temperature field under a new air delivery configuration.

The grid used in this study has a grid density of roughly 715 cells/m^3, which is smaller than grids from the literature by about 25%. Since the geometry and heat sources of this study are only *representative* of the actual test-facility, accurately simulating heat transfer is not the primary goal. Therefore, low y* values (~30) and detailed geometry are not necessary for a sufficiently good prediction of room temperature and velocity distribution. A basic grid sensitivity test was conducted to verify that a relatively coarse mesh produces stable results.

The sensitivity of spatial average vertical temperature profile to mesh density was investigated for the overhead mixing ventilation case. Grid refinement was done in increments of $\sqrt{2}$. When meshing, the size functions for all surfaces were changed such that the face meshes were larger/smaller and the growth rate was larger/smaller. The maximum cell edge length was set to 0.3 m, but never reached more than 0.23 m.

Table 19: Grid sensitivity number of cells

Grid	Number of Cells
Coarse	531,783
Medium	767,347
Fine	1,077,543

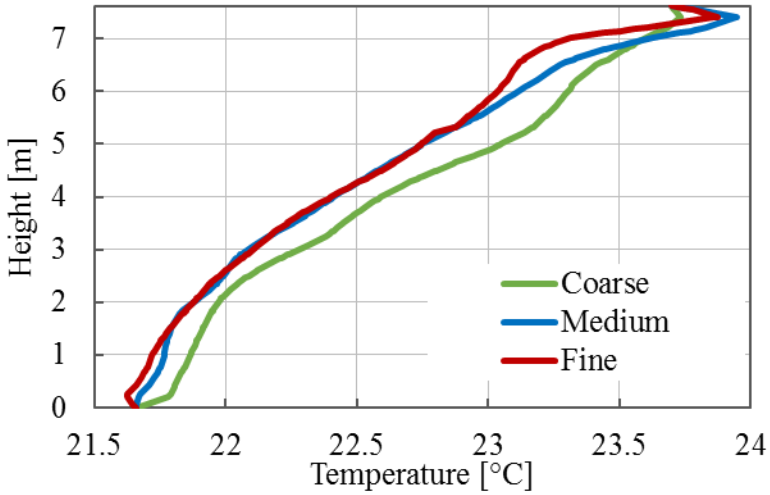

Figure 38: Grid sensitivity – vertical temperature profiles

The coarse grid over-predicted stratification everywhere except in the region 0.3 m from the ceiling. This region saw a larger temperature gradient when the mesh was refined. The edge length for the ceiling mesh was 0.229 m for the coarse mesh, 0.198 m for the medium mesh, and 0.183 m for the fine mesh. Temperature measurements were made at the ceiling surface (surface temperature) and 0.3 m below the ceiling. More measurements should be taken within 0-0.6 m from the ceiling to determine which mesh more accurately predicted heat transfer from the ceiling.

Since transient simulations were used for a steady-state problem (see Section 3.5 for convergence criteria), it is possible that the solution will have oscillations. The solution was taken at a time when the oscillations in the temperature field were small. However, the oscillations still impact the results slightly, which may explain the “S”

shape in the fine mesh's temperature profile, above, because this is the height at which the supply diffuser is located.

Since oscillatory convergence (in a transient sense), was observed, the grid convergence index (GCI) method proposed by Roache does not easily apply. Obviously, there exist formal grid convergence indices for transient studies. However, qualitative grid convergence was acceptable for this study. Since the medium mesh produces similar results to the fine mesh and has acceptable y* values, it was chosen as an appropriate mesh size for the remaining cases.

5.2.2 Model Validation

The CFD model was validated using the average vertical temperature profiles in the manufacturing room over the summer season. Since the time average temperature profile was used, the boundary conditions should be some time average as well. The boundary conditions for all heat transfer surfaces, like the walls, occupants, and machines, were discussed in Section 3.6.

The supply air velocity and temperature in the actual facility vary significantly between day and night. The RTU cycles on and off, as well as cycling between two flow rates. An appropriate boundary condition for supply temperature and flow rate was selected, then changed until the simulated average temperature profile matched the time averaged measured temperature profile.

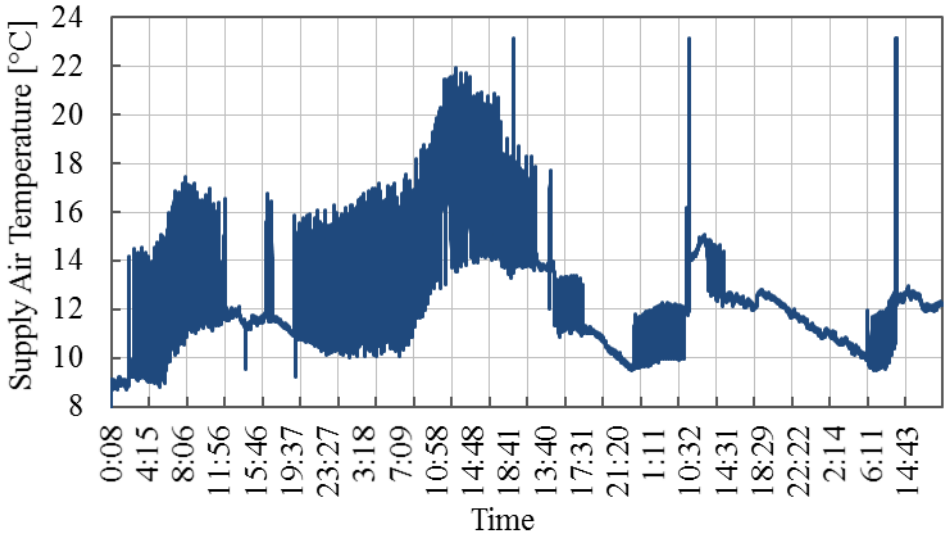

Figure 39: Measured supply air temperature of one RTU from 8/30/15 – 9/2/15 (note: some data is missing for this time period)

Based on Figure 39, the measured supply air temperature over the course of several days, the average supply air temperature is 12.7 ºC. During intermittent cooling, the temperature in the supply air duct cycles between about 11 ºC and 17 ºC. Flowrate is not measured, though this RTU has two nominal speeds: 2.6 m^3/s and 1.4 m^3/s Since there are times that the RTU is not supplying air, it is expected that the average supply air velocity is somewhere between 0 – 2.6 m^3/s. It was found through trial and error that 12 ºC and 0.56 m^3/s (2 m/s face velocity) provide a very accurate prediction of room air temperature for the baseline case. For the XChanger case, it was found that 14 ºC and 1.12 m^3/s (4 m/s face velocity) was best.

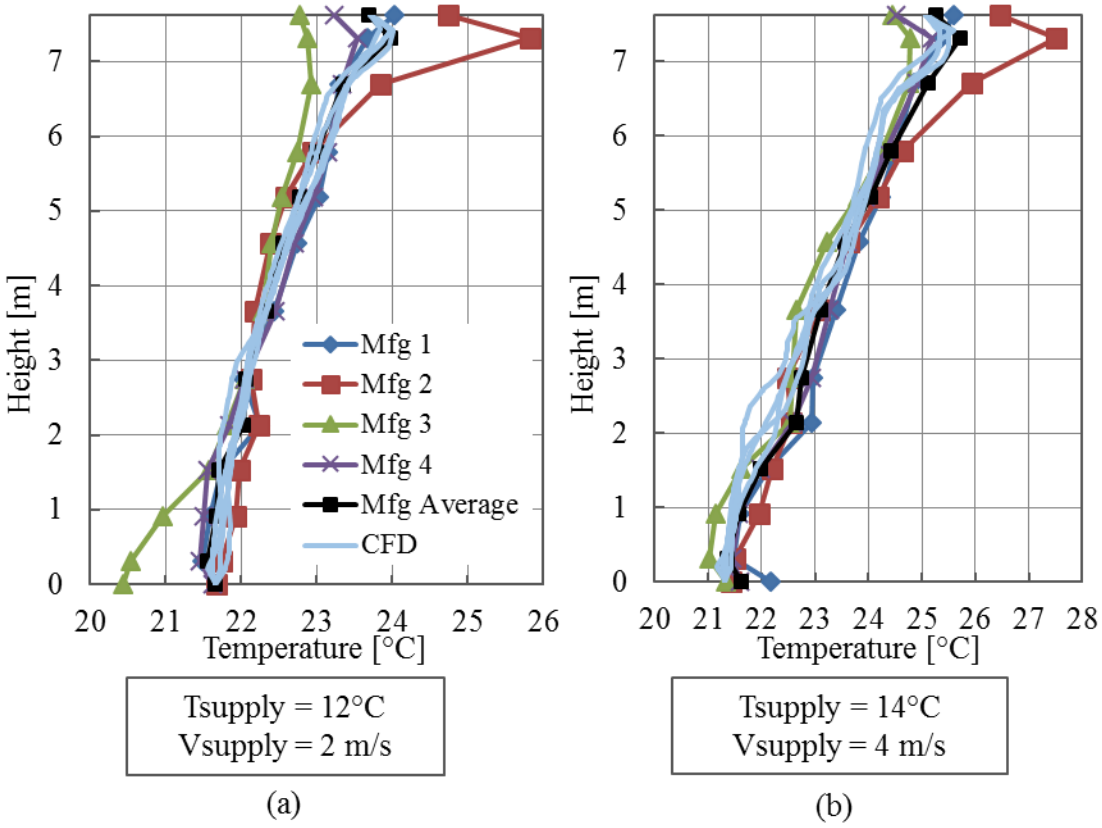

Figure 40: (a) Baseline and (b) XChanger CFD model validation

Figure 40 shows the model validation for vertical temperature profiles. The lines with markers are the thermocouple values at each pole in the large manufacturing room (averaged over the entire season). The black line is their average. The light blue lines are the temperature profiles along four lines in the flow domain, shown in Figure 41. Both cases were validated to within 0.2 ºC of the average measured profile. This is within measurement uncertainty, or 0.5 ºC.

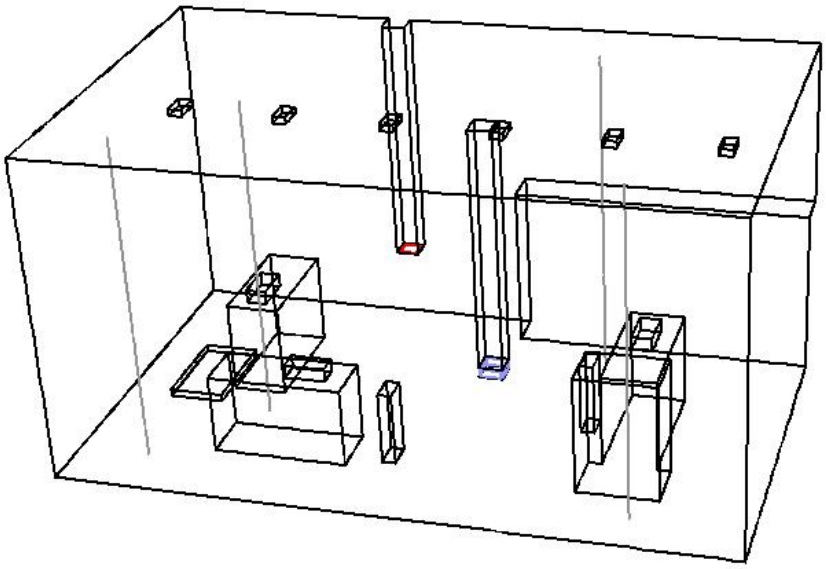

Figure 41: Vertical temperature profile measurement locations

Since the RTU was not changed, just the ducting, the supply air conditions should not change between baseline and XChanger cases significantly. The validated 'baseline boundary conditions' and the validated 'XChanger boundary conditions' were swapped to the opposite case. The results are plotted in Figure 42. The baseline model was over-cooled, which resulted in a uniform temperature distribution. The XChanger model velocity was too low, which resulted in over-cooling the occupied zone, a sharp temperature gradient between 1.5 m and 3 m, then uniform temperature between 3 m and the ceiling.

It was not expected that the solution would be so sensitive to supply air conditions. For example, the temperature profile from the XChanger case in Figure 42 has entirely different features than Figure 41 due to a 2 ºC decrease in temperature and decreasing the velocity by a factor of two. Since a satisfactory explanation for this sensitivity has not been found and it is unclear which set of boundary conditions to proceed with, both sets of boundary conditions will be used for the parametric

study.

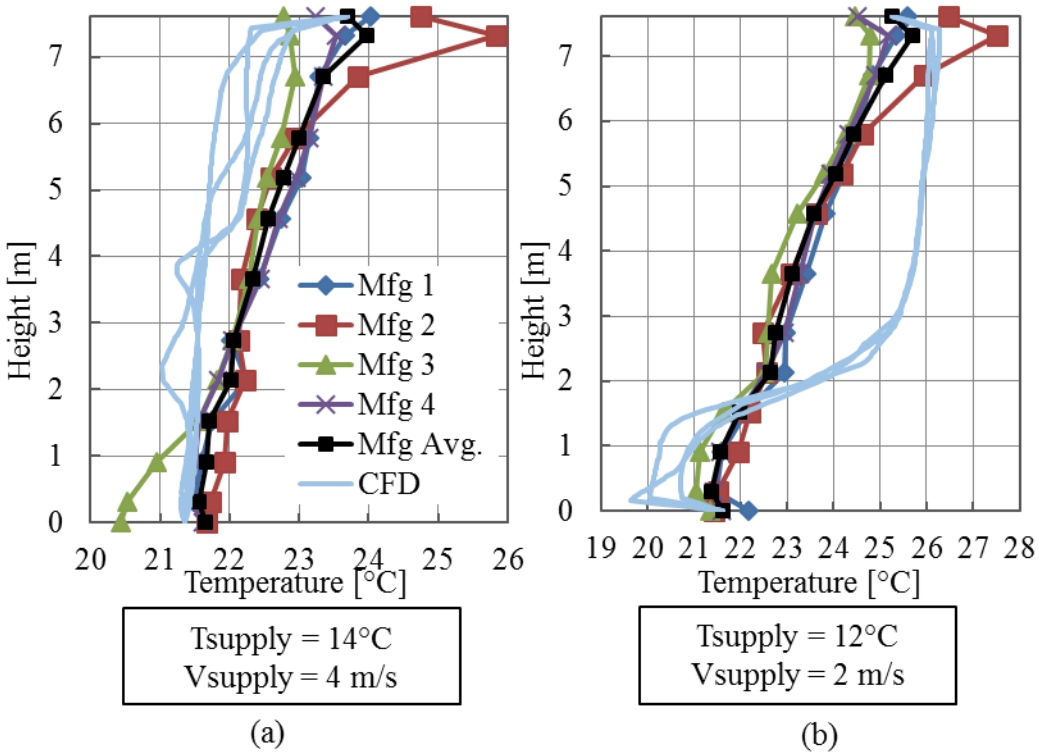

Figure 42: (a) Baseline and (b) XChanger with the opposite boundary conditions

5.2.3 Parametric Study

Each case below is simulated with the baseline and XChanger boundary conditions, hereby referred to as 'low velocity' and 'high velocity', respectively.

Table 20: Parametric study test matrix

Case	Description	Supply Height [m]	Return Height [m]
Baseline	Overhead, mixing ventilation	7.0	7.0
XChanger	As installed	1.8	2.4
Case 1	"Preferred" installation	0.46	2.4
Case 2	Higher Return	1.8	5.5
Case 3	Double face area	0.46	2.4

Case 1 has the supply duct at the same height as the installed XChanger, but the return duct is located at two-thirds height, instead of one-third. Case 2 is how the

XChanger company prefers to install units – supply near the floor and return just above the occupied zone. Case 3 investigates a doubling of the supply air diffuser face area and the corresponding decrease in inlet velocity.

A user-defined function in Fluent was created to calculate PMV and PPD according to ISO-7730, which is the same as ASHRAE Standard 55 without the SET model (Standard Effective Temperature). It is assumed that the relative humidity is 50%, the clo value is 0.6 (the uniform of the workers), the metabolic rate is 2 met (typical of light machine work), and the radiant temperature is the same as the air temperature. This choice of metabolic rate is rather high compared to typical office settings and resulted in the occupants feeling slightly warm.

Table 21 lists results for the parametric study. Each value is averaged over the entire flow domain. The 'high velocity' supply air boundary conditions (those found for the XChanger case validation) were more appropriate for each of the three cases because the low velocity boundary conditions resulted in significant stratification – similar to the stratification seen on the right in Figure 42. Therefore, most analysis will only consider the cases with 'high velocity' boundary conditions. The stratification is taken as the average temperature difference between 0.2 m from the floor and 0.2 m from the ceiling – where the lowest and highest temperatures are usually observed.

Increasing the return duct height in Case 2 compared to the XChanger case has the effect of reducing the average temperature in the space, reducing stratification (particularly in the upper zone), and increasing the return air temperature. Case 1, supplying at floor-level and returning at the same height as the installed XChanger,

shows an average temperature reduction of 0.4 K, a reduction in stratification of 0.8 K, and an increase in return air temperature comparable to Case 1. Supplying air near the floor while increasing the supply diffuser area has the effect of greatly increasing stratification and slightly increasing average air temperature.

Table 21: Parametric study results (averages over entire flow domain)

Whole Volume						
Case	Temp. [ºC]	Velocity [m/s]	PMV [-]	PPD [%]	RAT [ºC]	Stratification [K]
Baseline	22.5	0.11	0.6	14.2	22.0	2.3
XChanger	23.2	0.12	0.7	18.8	21.8	4.5
Case 1 Low Velocity	24.2	0.08	1.0	28.0	24.4	4.6
Case 1 High Velocity	22.8	0.11	0.7	16.7	22.3	3.7
Case 2 Low Velocity	23.5	0.07	0.8	21.7	24.5	6.8
Case 2 High Velocity	22.1	0.13	0.5	12.8	22.6	3.9
Case 3 Low Velocity	24.2	0.07	1.0	29.1	24.5	8.0
Case 3 High Velocity	23.1	0.07	0.7	20.9	22.6	6.3

Energy savings can generally be achieved by increasing the average air temperature of the space, which decreases heat gain through the building envelope. It would be misleading to simply point out which case in Table 21 saves the most energy based on this criteria because these simulations have no concept of thermostat control. In other words, a thermostat would control the room temperature such that the temperature near the thermostat is at set point. In the simulation, the temperature near the thermostat is not controlled. A better way to express the effect of average air temperature is the difference between mean air temperature and temperature near the location of a typical thermostat: 1.5 m height on the wall. This value expresses the increase in mean air temperature from setpoint that a room would expect to see under each case.

Based on Table 22, Case 3 would have the least heat gain from ambient due to the excessive stratification and the baseline case would have the most heat gain from ambient due to mixing. In Case 3, the high velocity case saw both a higher mean air temperature and a lower thermostat temperature because the supply air jet reached the wall (and this is where the thermostat would be located). The thermal comfort implications of this need to be investigated.

Table 22: Average temperature minus hypothetical thermostat temperature

Case	$T_{avg} - T_{thermostat}$
Baseline	0.64
XChanger	1.81
Case 1 Low Velocity	3.20
Case 1 High Velocity	2.00
Case 2 Low Velocity	1.38
Case 2 High Velocity	1.31
Case 3 Low Velocity	1.92
Case 3 High Velocity	3.73

According to ASHRAE Standard 55-2013, the occupied zone is the region that is 10 cm off the ground, below 1.8 m, and 0.3 m away from the walls. Table 23 shows the average values of several parameters over this region.

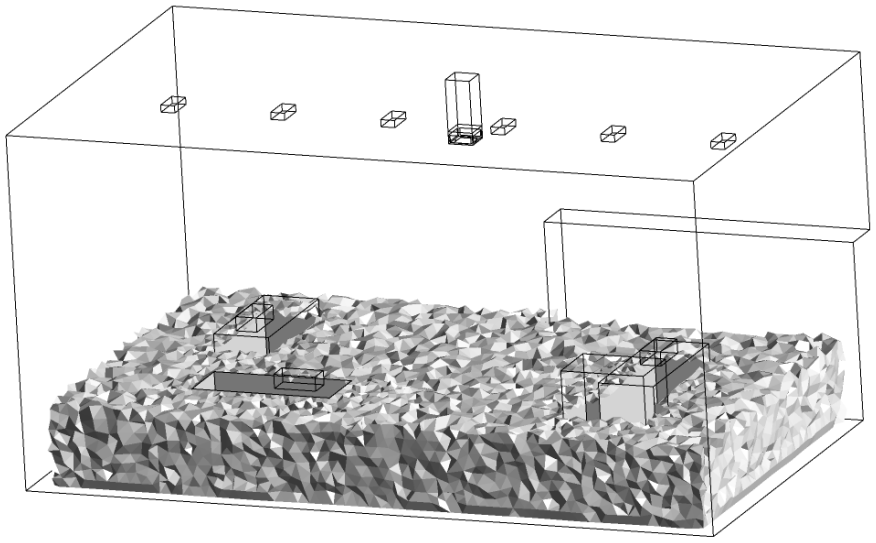

Figure 43: ASHRAE definition of occupied zone

Table 23: Parametric study results; averages over the occupied zone

Occupied Zone					
Case	Temperature [ºC]	Velocity [m/s]	PMV [-]	PPD [%]	Head-to-Ankle [ºC]
Baseline	21.81	0.13	0.49	10.45	0.30
XChanger	21.51	0.20	0.39	9.12	0.38
Case 1 Low Velocity	20.30	0.13	0.21	8.53	3.59
Case 1 High Velocity	20.93	0.24	0.26	8.42	0.88
Case 2 Low Velocity	20.75	0.14	0.29	7.61	0.66
Case 2 High Velocity	20.89	0.20	0.27	7.40	0.21
Case 3 Low Velocity	19.90	0.09	0.16	8.79	4.89
Case 3 High Velocity	19.39	0.18	0.00	7.20	1.49

The average particular mean vote (PMV) and percent people dissatisfied (PPD) are within acceptable ranges for each case considered. The baseline, mixing ventilation had the most dissatisfied occupants, but by a negligible amount. ASHRAE Standard 55 specifies that the head-to-ankle temperature difference be less than 3 °C for seated occupants and 4 °C for standing occupants. Each case except the low-velocity, large-diffuser case satisfied this criteria. Figure 44 shows contour plots for

each high velocity case in the plane of the supply diffuser. Although the ISO 7730:2005 thermal comfort model was intended for use in spaces with uniform conditions, it is useful here to qualitatively view comfort.

The baseline case has uniform PPD less than 20% in the entire space. Clearly, the other cases have PPD approaching 100% near the supply diffusers, yet acceptable PPD outside the vicinity of the diffuser. Moreover, the large area diffuser, Case 3, does not have an appreciable drop in PPD near the diffuser. Therefore, care should be taken during installation to aim the diffuser away from occupants.

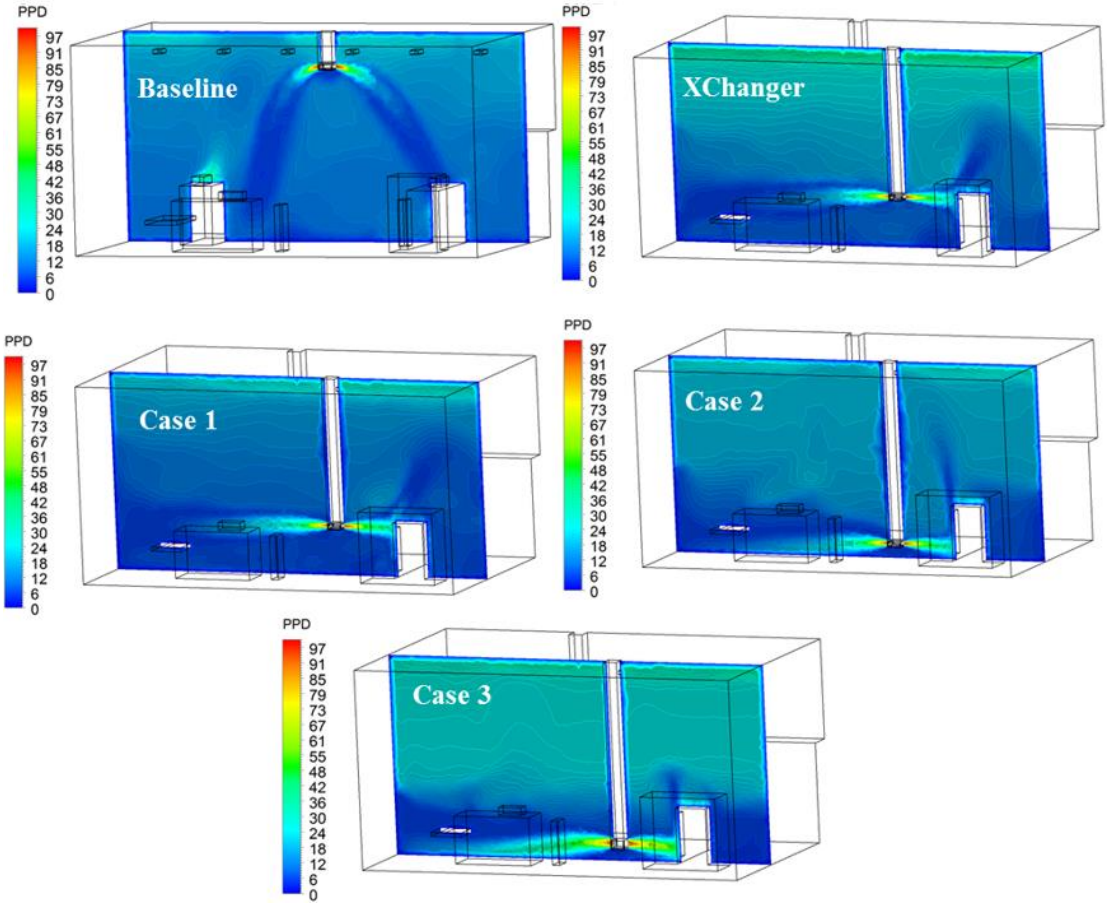

Figure 44: PPD contours for each case (only high velocity cases shown)

5.3 EnergyPlus Modeling

5.3.1 Model Validation

An EnergyPlus model was created for 2015 that contains each building retrofit – lighting, RTUs, XChanger, and the new air compressor. This model has been validated using daily site electricity use and monthly gas use. According to ASHRAE Guideline 14, normalized mean bias error (NMBE) and coefficient of variation of root mean square error (CVRSME) should be within the range specified in Table 24.

Table 24: ASHRAE guideline 14 requirements

	NMBE [%]	CV(RSME) [%]
Hourly data	< 10	< 30
Daily data	Not specified	Not specified
Monthly data	< 5	< 15

Table 25: 2015 EnergyPlus model calibration statistics

Variable	NMBE [%]	CV(RSME) [%]
Electricity (daily)	-0.27	7.75
Gas (monthly)	2.04	22.84

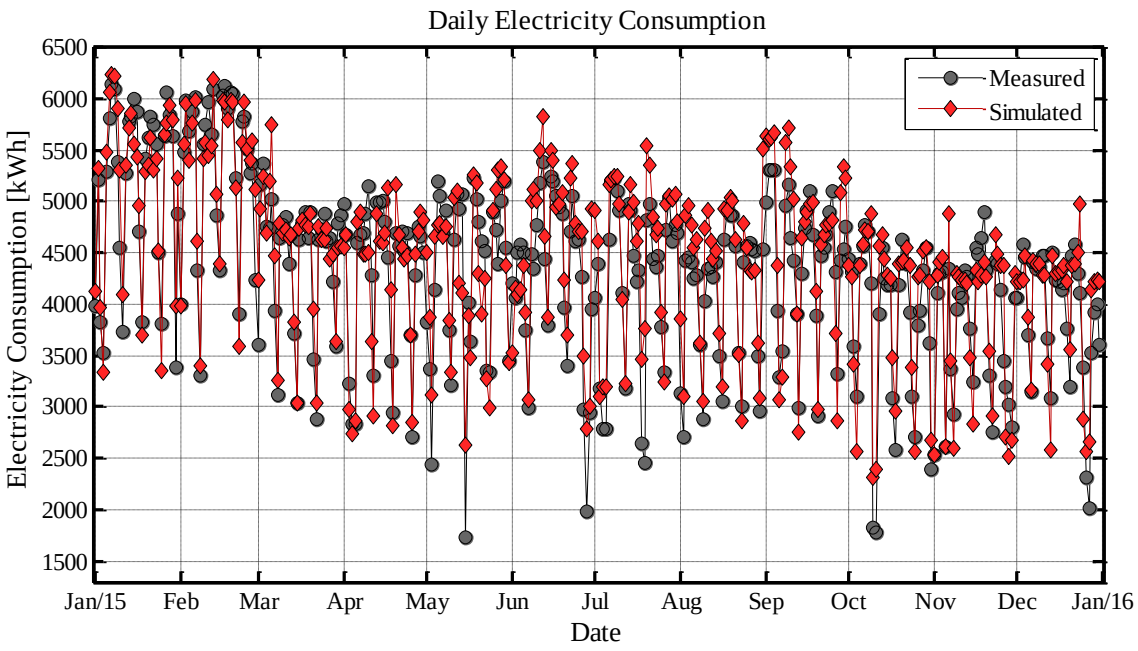

Figure 45: Model versus measured daily electricity use

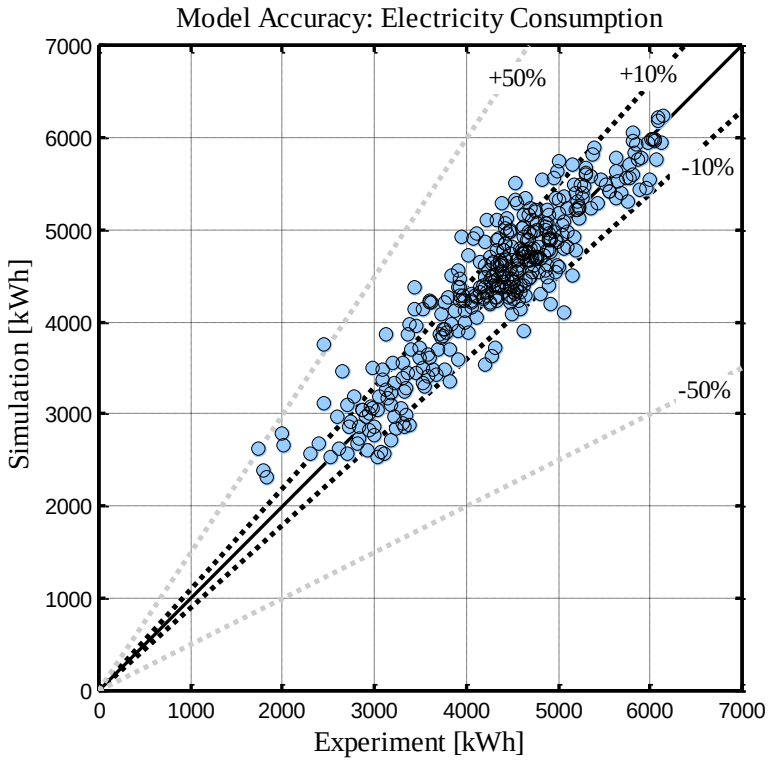

Figure 46: Accuracy of simulated daily electricity consumption

The model accurately predicts electricity use, as shown in the above three figures. The NMBE and CV(RSME) values are within the ASHRAE specified range except for the CV(RSME) value for gas. As shown in Figure 45, the model slightly over-predicts electricity use in the summer and under-predicts electricity use in the winter.

Before calibration, the model significantly over-predicted summer electricity. This was addressed by decreasing the plug load by a factor of 2 between May 4 and August 30. It is believed that the manufacturing output may be less during the summer than during the rest of the year. One piece of justification for this theory is the sudden increase in measured facility electricity on the first week in September.

Before calibration, the model also significantly under-predicted winter electricity. This was accounted for by increasing the capacity of the VAV reheat for the offices, because this is the only source of electric heating in the facility. The actual capacity or number of VAV boxes is not known, but was assumed based on the number and size of offices. The significant under-prediction of gas use in February and March and the over-prediction of gas use in September prevent the model from being considered calibrated.

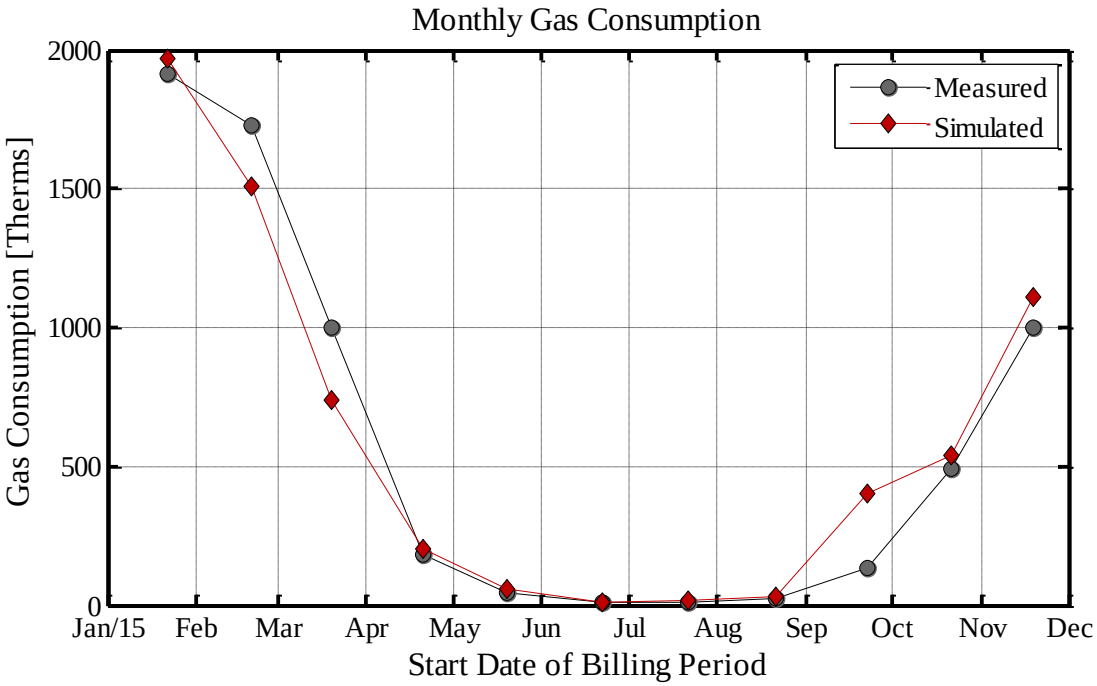

Figure 47: Simulated and measured monthly gas use

5.3.2 Energy Savings of Proposed System

Two models were created based on the validated 2015 model – one with all measured baseline temperature profiles and one with all measured XChanger temperature profiles. The set point offset was also changed to correspond with the appropriate temperature profiles (see Room Air Modeling). The temperature profile used for each time period in each model is shown in Table 26. The names of the temperature profiles correspond to the legend in Figure 34.

Table 26: Temperature profile corresponding to model and time period

Period	Mixing ventilation model	XChanger model
1/1 – 3/23	Baseline Winter	XChanger Winter
3/24 – 5/31	Baseline Spring	XChanger Fall
6/1 – 9/22	Baseline Summer	XChanger Summer
9/23 – 11/31	Baseline Spring	XChanger Fall
12/1 – 12/31	Baseline Winter	XChanger Winter

The XChanger adds additional ducting and several 90 degree elbows, as discussed in Section 4.7.4. Therefore, fan static pressure rise will be greater in the 'all XChanger' model compared with the baseline model. Since fan energy consumption is the same order of magnitude as cooling coil energy consumption, which is common for commercial buildings, the increased fan power could dominate the energy savings due to stratification. For this reason, it is necessary to handle fan static pressure rise accurately.

Two EnergyPlus models were created to show the sensitivity of fan power consumption – one with equal pressure drop between baseline and XChanger and another with the pressure drops calculated in Section 4.7.4. The fans used in the first two models were *Fan:VariableVolume* objects. These fans never fully turn off – they just operate at their minimum part load ratio when demand is low. One problem with these models is that fan static pressure rise is defined at the fan's nominal flow rate, not as a function of air flow rate. This fact leads to large fan power consumption at part load. Additionally, the fans do not cycle with coil operation, which is how the real RTU operates. Table 27 shows each model's details.

Table 27: Models used to compare fan controls and static pressure rise

Model	Description
1	XChanger and baseline systems have the same pressure drop
2	$\Delta P_{Baseline}$ = 144.5 Pa, $\Delta P_{XChanger}$= 248.4 Pa

The calculated HVAC energy savings of XChanger are shown in Table 28. When fan power consumption is the same in baseline and XChanger models,

stratification alone saves 37.4% electricity and 7.7% gas. In other words, these savings are realized by the room air modeling temperature profiles, return air offset, and thermostat offset. When factoring fan pressure drop into the model, the savings dropped to 19.3% electricity. The gas savings increased because the added heat of the fans required less gas to be burned and should therefore not be considered a benefit. As a percentage of the total facility electricity (i.e. not just HVAC energy), Model 1 shows a 5.0% electricity savings and Model 2 shows a 2.2% electricity savings.

Table 28: Energy savings of XChanger based on EnergyPlus models

Model	HVAC Electricity Savings [%]	Gas Savings [%]
1	37.4	7.7
2	19.3	25.2

6. Conclusions

A full-scale experiment was conducted in a high-bay test facility to measure the effects of a new air delivery strategy. The experimental study shows that, in cooling, supplying and returning air directly to the occupied zone produces an acceptable temperature gradient in the occupied zone, while increasing stratification in the upper portion of the space. In heating, supplying air from the ceiling vertically downward while returning air in the occupied zone has the potential to reduce stratification, though not eliminate it entirely. In both heating and cooling, the effects of the installed system are more pronounced in rooms that have high cooling and heating loads.

CFD modeling reveals the effects of supply and return duct location on room air flow and stratification generation. Supplying air lower generally creates more stratification and an acceptable temperature gradient in the occupied zone. Increasing the supply diffuser face area while holding flow rate constant produces lower velocities in the occupied zone, creates large temperature gradients in the occupied zone, and produces the largest stratification observed. The room temperature gradient is less sensitive to return duct height than supply duct height, though increasing the return duct height slightly reduced stratification and the average room temperature.

Building energy simulation is used to show how stratification influences a building's energy use. A novel approach used room air modeling with 24 measured temperature profiles over one year to capture the effects of return air temperature offset, thermostat offset, and stratification. It was found that increased fan energy

consumption due to the XChanger system's larger pressure drop can depreciate the energy savings by 50%.

Based on the utility bill analysis and measured combined RTU power consumption, XChanger saves the facility 28.8% HVAC electricity over the course of one year. The EnergyPlus models bracket this result – not accounting for pressure drop resulted in 37.4% HVAC electricity savings while accounting for pressure drop resulted in 19.3% HVAC electricity savings. Building simulation results would be closer to experimental results if the fans in EnergyPlus were simulated more realistically (i.e. had pressure drop as a function of flow rate, not specified at the fan's nominal flow rate).

Gas consumption results for the experiment are inconclusive because the same therm-per-degree-day value was calculated before and after XChanger was switched to heating mode. Also, "savings" in terms of therm-per-degree-day were observed before any retrofits took place. These unexpected results are observed because the heating load in the space changed due to the other three retrofits over the measurement period. Attempts were made to 'add back' the heat of these retrofits but this approach adds uncertainty. Building energy simulation shows that XChanger saves 7.7 – 25.2% gas, depending on fan power consumption.

7. Future Work

For this experiment, detailed measurement of RTU power consumption was too costly due to the number of RTUs. Additionally, the effects of three retrofits in addition to the XChanger system adds uncertainty to the calculated energy savings because one must attribute a certain percentage of the energy savings to each retrofit.

Therefore, a future version of this study should be conducted on a simpler building, where detailed RTU power consumption is measured before and after the ducting retrofit. That retrofit should be the only retrofit installed in the entire facility. Sub-hourly metering in addition to measured temperature profiles may provide insight into observed differences between the building energy simulation results and measured results.

The effects of duct height during heating operation should be investigated using CFD simulation to answer the following questions: Does returning air in the occupied zone draw air down, reducing stratification? Should air instead be both supplied and returned in the occupied zone? If so, should the supply velocity be increased to induce thermal mixing in the occupied zone?

Building energy simulation using room air modeling can address the possibility of using different supply air conditions with different ducting configurations. This would bridge the gap between this thesis and research in the literature regarding displacement ventilation and underfloor air distribution. Also, since the fan pressure drop has been shown to be a significant degradation of the XChanger's energy saving potential, the work in this thesis should include more accurate fan models, such as the *Fan:ComponentModel* approach.

References

Alajmi, Ali, and Wid El-Amer. 2010. “Saving Energy by Using Underfloor-Air-Distribution (UFAD) System in Commercial Buildings.” *Energy Conversion and Management*, Global Conference on Renewables and Energy Efficiency for Desert Regions (GCREEDER 2009), 51 (8): 1637–42. doi:10.1016/j.enconman.2009.12.040.

“ANSYS Fluent Users Guide.pdf.” 2016. Accessed February 27.

“ASHRAE Standard 55 - 2013.” 2013. American Society of Heating a Refrigeration Engineers.

“ASHRAE Standard 90.1.” 2007. American Society of Heating a Refrigeration Engineers.

Aynsley, Richard. 2005. “Saving Heating Costs in Warehouses.” *ASHRAE Journal* 47 (12): 46–51.

Cheng, Yuanda, Jianlei Niu, and Naiping Gao. 2012a. “Thermal Comfort Models: A Review and Numerical Investigation.” *Building and Environment*, International Workshop on Ventilation, Comfort, and Health in Transport Vehicles

Cheng, Yuanda, Jianlei Niu, and Naiping Gao. 2012b. “Stratified Air Distribution Systems in a Large Lecture Theatre: A Numerical Method to Optimize Thermal Comfort and Maximize Energy Saving.” *Energy and Buildings*, Cool Roofs, Cool Pavements, Cool Cities, and Cool World

Chen, Qingyan. 1990. “Prediction of Buoyant, Turbulent Flow by a Low-Reynolds-Number K-Epsilon Model.” *ASHRAE Transactions*, vol. 96, 1990.

Chen, Qingyan.. 1995. “Comparison of Different K-ε Models for Indoor Air Flow Computations.” *Numerical Heat Transfer, Part B Fundamentals* 28 (3): 353–69.

Chen, Q., and Z. Zhai. 2004. “The Use of CFD Tools for Indoor Environmental Design.” *Advanced Building Simulation*, 119–40.

Efficiency, Energy, and Department of Energy. 2013. “Improving Compressed Air System Performance.”

EIA. 2015. "U.S. Energy Information Administration - EIA - Independent Statistics and Analysis." CBECS 2012: Building Stock Results. March 4, 2015. Accessed January 13, 2016.

"Fluent User's Guide - ANSYS Fluent Users Guide.pdf." 2016. Accessed February 27.

Gilani, S., H. Montazeri, and B. Blocken. 2013. "CFD Simulation of Temperature Stratification for a Building Space: Validation and Sensitivity Analysis." In *Proceedings of BS2013: 13th Conference of International Building Performance Simulation Association, Chambéry, France, August*, 26–28.

Gowri, Krishnan, David W. Winiarski, and Ronald E. Jarnagin. 2009. *Infiltration Modeling Guidelines for Commercial Building Energy Analysis*. Pacific Northwest National Laboratory USA.

Griffith, Brent. 2002. "Incorporating Nodal and Zonal Room Air Models into Building Energy Calculation Procedures." MIT.

Griffith, Brent, and Qingyan Yan Chen. 2003. "A Momentum-Zonal Model for Predicting Zone Airflow and Temperature Distributions to Enhance Building Load and Energy Simulations." *HVAC&R Research* 9 (3): 309–25.

Griffith, Brent, and Qingyan Yan Chen. 2004. "Framework for Coupling Room Air Models to Heat Balance Model Load and Energy Calculations (RP-1222)." *HVAC&R Research* 10 (2): 91–111.

Hajdukiewicz, Magdalena, Marco Geron, and Marcus M. Keane. 2013a. "Formal Calibration Methodology for CFD Models of Naturally Ventilated Indoor Environments." *Building and Environment* 59 (January): 290–302.

Hajdukiewicz, Magdalena, Marco Geron, and Marcus M. Keane. 2013b. "Calibrated CFD Simulation to Evaluate Thermal Comfort in a Highly-Glazed Naturally Ventilated Room." *Building and Environment* 70 (December): 73–89.

Hawileh, Rami A. 2011. *Heat Transfer Analysis of Reinforced Concrete Beams Reinforced with GFRP Bars*. INTECH Open Access Publisher.

"ISO 7730:2005 - Ergonomics of the Thermal Environment -- Analytical Determination and Interpretation of Thermal Comfort Using Calculation of the

PMV and PPD Indices and Local Thermal Comfort Criteria." 2016. Accessed January 18.

Jones, P.J., and G.E. Whittle. 1992. "Computational Fluid Dynamics for Building Air Flow Prediction - Current Status and Capabilities." *Building and Environment* 27 (3): 321–38.

McQuiston, Parker, and Spitler. 2004. *Heating, Ventilating and Air Conditioning Analysis and Design*. 6 edition. Hoboken, N.J: Wiley.

Nielsen, Peter V., and Tryggvi Tryggvason. 1998. "Computational Fluid Dynamics and Building Energy Performance Simulation." Dept. of Building Technology and Structural Engineering.

Pan, Yiqun, Yuming Li, Zhizhong Huang, and Gang Wu. 2010. "Study on Simulation Methods of Atrium Building Cooling Load in Hot and Humid Regions." *Energy and Buildings* 42 (10): 1654–60.

Pedersen, Curtis, Daniel Fisher, and Richard Liesen. 1997. "Devolopment of a Heat Balance Procedure for Calculating Cooling Loads." In . Vol. 103 Part 2.

Risberg, Daniel, Mattias Vesterlund, Lars Westerlund, and Jan Dahl. 2015a. "CFD Simulation and Evaluation of Different Heating Systems Installed in Low Energy Building Located in Sub-Arctic Climate." *Building and Environment* 89 (July): 160–69.

Risberg, Daniel, Mattias Vesterlund, Lars Westerlund, and Jan Dahl .2015b. "CFD Simulation and Evaluation of Different Heating Systems Installed in Low Energy Building Located in Sub-Arctic Climate." *Building and Environment* 89 (July): 160–69.

Risberg, Daniel, Lars Westerlund, and Gunnar JI Hellström. 2015. "CFD-Simulation of Indoor Climate in Low Energy Buildings Computational Setup." *Thermal Science*, no. 00: 167–167.

Roache, Patrick J. 1997. "Quantification of Uncertainty in Computational Fluid Dynamics." *Annual Review of Fluid Mechanics* 29 (1): 123–60.

Rohdin, P., and B. Moshfegh. 2011. "Numerical Modelling of Industrial Indoor Environments: A Comparison between Different Turbulence Models and Supply

Systems Supported by Field Measurements." *Building and Environment* 46 (11): 2365–74.

Saïd, M. N. A., R. A. MacDonald, and G. C. Durrant. 1996. "Measurement of Thermal Stratification in Large Single-Cell Buildings." *Energy and Buildings* 24 (2): 105–15.

Sheppy, Michael, Paul Torcellini, and Luigi Gentile-Polese. 2014. "An Analysis of Plug Load Capacities and Power Requirements in Commercial Buildings." National Renewable Energy Laboratory (NREL), Golden, CO.

Singh, Trilochan, and J. B. Olivieri. 1988. "Thermal Stratification-A Means to Reduce Cooling Loads in High Bay Industrial Buildings."

Sørensen, D. N., and P. V. Nielsen. 2003. "Quality Control of Computational Fluid Dynamics in Indoor Environments." *Indoor Air* 13 (1): 2–17.

Srebric, Jelena. 2000. "Simplified Methodology for Indoor Environment Designs." Massachusetts Institute of Technology.

Srebric, Jelena, and Qingyan Chen. 2002. "Simplified Numerical Models for Complex Air Supply Diffusers." *HVAC&R Research* 8 (3): 277–94.

Srebric, Jelena, Qingyan Chen, Ph D. Leon R. Glicksman, and others. 2000. "A Coupled Airflow-and-Energy Simulation Program for Indoor Thermal Environment Studies (RP-927)." *ASHRAE Transactions* 106 (1): 465–76.

Topp, Claus, Peter V. Nielsen, and Dan Sorensen. 2002. "Application of Computer Simulated Persons in Indoor Environmental Modeling / Discussion." *ASHRAE Transactions* 108: 1084.

Tsai, Ting-Ya, Ren-Hao Liou, and Yi-Jiun Peter Lin. 2014. "An Experimental Study on the Indoor Environment Using UnderFloor Air Distribution System." *Procedia Engineering*, 37th National Conference on Theoretical and Applied Mechanics (37th NCTAM 2013) & The 1st International Conference on Mechanics (1st ICM), 79: 263–66.

Wang, Xin, Chen Huang, Weiwu Cao, Xuelei Gao, and Wen Liu. 2011. "Experimental Study on Indoor Thermal Stratification in Large Space by under

Floor Air Distribution System (UFAD) in Summer." *Engineering* 03 (04): 384–88.

Wang, Yang, Jens Kuckelkorn, Fu-Yun Zhao, Mu-Lan Mu, and Hartmut Spliethoff. 2014. "Indoor Air Environment and Heat Recovery Ventilation in a Passive School Building: A Case Study for Winter Condition." *ASHRAE Transactions* 120: TT1–8.

Wetter, Michael, and Christoph Haugstetter. 2006. "Modelica versus TRNSYS–A Comparison between an Equation-Based and a Procedural Modeling Language for Building Energy Simulation." In *Proc. of the SimBuild, 2nd National Conference of IBPSAUSA*.

Woods, James E. 2004. "What Real-World Experience Says about the UFAD Alternative." *ASHRAE Journal* 46 (2): 3–13.

"XChanger Companies, Inc." 2016. http://xcoinc.net/.

Yuan, Xiaoxiong, Qingyan Chen, and Leon Glicksman. 1999. "Measurements and Computations of Room Airflow with Displacement Ventilation." *ASHRAE Transactions* 105: 340.

Zhai, Zhiqiang, and Qingyan (Yan) Chen. 2003. "Solution Characters of Iterative Coupling between Energy Simulation and CFD Programs." *Energy and Buildings* 35 (5): 493–505.

Zhai, Zhiqiang, Zhao Zhang, Wei Zhang, and Qingyan Chen. 2007. "Evaluation of Various Turbulence Models in Predicting Airflow and Turbulence in Enclosed Environments by CFD: Part-1: Summary of Prevalent Turbulence Models." *HVAC&R Research* 13 (6).

Zhang, Zhao, Wei Zhang, Zhiqiang John Zhai, and Qingyan Yan Chen. 2007. "Evaluation of Various Turbulence Models in Predicting Airflow and Turbulence in Enclosed Environments by CFD: Part 2—Comparison with Experimental Data from Literature." *HVAC&R Research* 13 (6): 871–86.